

Multi-Static Target Detection and Power Allocation for Integrated Sensing and Communication in Cell-Free Massive MIMO

Zinat Behdad, Özlem Tuğfe Demir, Ki Won Sung,

Emil Björnson, and Cicek Cavdar

Abstract

This paper studies an integrated sensing and communication (ISAC) system for single-target detection in a cloud radio access network architecture. The system considers downlink communication and multi-static sensing approach, where ISAC transmit access points (APs) jointly serve the user equipments (UEs) and optionally steer a beam toward the target. A centralized operation of cell-free massive MIMO (multiple-input multiple-output) is considered for communication and sensing purposes. A maximum a posteriori ratio test detector is developed to detect the target in the presence of clutter, so-called target-free signals. Moreover, a power allocation algorithm is proposed to maximize the sensing signal-to-interference-plus-noise ratio (SINR) while ensuring a minimum communication SINR value for each UE and meeting per-AP power constraints. Two ISAC setups are studied: i) using only existing communication beams for sensing and ii) using additional sensing beams. The proposed algorithm's efficiency is investigated in both realistic and idealistic scenarios, corresponding to the presence and absence of the target-free channels, respectively. Although detection probability degrades in the presence of target-free channels that act as interference, the proposed algorithm significantly outperforms the interference-unaware benchmark by exploiting the statistics of the clutter. It has also been shown that the proposed algorithm outperforms the fully communication-centric algorithm, both in the presence and absence of clutter. Moreover, using an additional sensing beam improves the detection performance for a target with lower radar cross-section variances compared to the case without sensing beams.

Index Terms

Integrated sensing and communication (ISAC), cell-free massive MIMO, C-RAN, power allocation, multi-static sensing.

Z. Behdad, K. W. Sung, E. Björnson, and C. Cavdar are with the Department of Computer Science, KTH Royal Institute of Technology, Kista, Sweden (`{zinatb, sungkw, emilbjo, cavdar}@kth.se`). Ö. T. Demir is with the Department of Electrical and Electronics Engineering, TOBB University of Economics and Technology, Ankara, Turkey (`ozlemtugfedemir@etu.edu.tr`). Results incorporated in this paper received funding from the ECSEL Joint Undertaking (JU) under grant agreement No 876124. The JU receives support from the EU Horizon 2020 research and innovation programme and Vinnova in Sweden.

I. INTRODUCTION

Radio-based positioning and sensing have gained considerable attention as one of the key enablers in beyond 5G and 6G wireless networks. It is envisioned that integrated sensing and communication (ISAC), also known as joint sensing and communication (JSAC), will become a promising technology in future wireless systems, providing many sensing applications [1] [2]. It is expected to support various use cases, including remote healthcare, remote monitoring of weather conditions, asset tracking, gesture recognition, autonomous vehicles, and augmented reality (AR). The main idea of such a system is to share infrastructure, resources, and signals between communications and sensing to improve the spectral efficiency and sensing performance while lowering the hardware and deployment costs [2]–[7]. The communication performance could also be enhanced by exploiting the sensing information to estimate the channel and optimize the network steering [8]. ISAC benefits from current developments in wireless systems, i.e., denser access point (AP) deployment and wider bandwidths [2]–[4].

From the network-level perspective, ISAC is expected to provide a ubiquitous radar perception system [9]–[11], also known as a *perceptive mobile network* [12]. The focus of the research on ISAC has been mainly on waveform design and signal processing (see [7]–[9], [13]–[22]), in which ISAC is mostly considered in single-cell scenarios with mono-static sensing, which refers to a co-located transmitter and receiver for sensing. Bi-static sensing, involving a non-co-located transmitter and receiver, can be employed to dispense with the full-duplex capability requirement in mono-static sensing. Multi-static sensing, which uses multi non-co-located transmitters and receivers, can also be preferable since it provides a diversity gain due to multiple uncorrelated sensing observations at distributed sensing receivers. Furthermore, multi-static sensing offers an additional performance gain as it achieves increased joint transmit/receive beamforming gain by using multiple transmitters/receivers in the network.

To implement multi-static sensing in an existing communication system, cell-free massive MIMO (cell-free massive multiple-input multiple-output) is a promising infrastructure [23], which motivates our work. To fully realize the advantages of cell-free massive MIMO, it is preferred to use phase-coherent centralized joint processing. This involves implementing transmit/receive processing by utilizing all the channel estimates obtained from each access point (AP) and processing them in a central processing unit. The cloud radio access network (C-RAN) architecture facilitates centralization and synchronization among the distributed APs [24]. This architecture has recently gained interest in ISAC systems [11].

There is usually a trade-off between sensing and communication performance due to the shared resources (e.g., time, frequency, power, and space). This trade-off can be balanced by exploiting the existing communication signals for sensing purposes or integrating sensing signals by guaranteeing a specific communication performance. Despite the progress made in this area, there is still a need for new processing and resource allocation schemes that can effectively address both communication and sensing requirements. This becomes even more challenging in cell-free ISAC with joint transmission/reception.

This work studies the detection of a single target in a cell-free ISAC system in the presence of clutter and imperfect channel state information (CSI). The clutter refers to the undesired received signals such as reflections from non-target objects. It can be treated as interference for sensing and will affect the performance of target detection. In this paper, the clutter is characterized by the unknown components of the channels between the ISAC transmitter and sensing receiver APs. However, the communication symbols contribute to sensing by the reflected paths toward the target. Therefore, these reflections are not considered as interference. This is why we design the precoding vectors so that we null the interference only for UEs. A power allocation algorithm is proposed to effectively maximize the sensing performance while ensuring that the communication performance remains satisfactory. The preliminary results for a simple channel model with perfect CSI for the communication and sensing channels, without considering clutter, have been published in [25].

A. Related Work

Table I presents an overview of some of the research conducted on ISAC.¹ The table highlights that a few papers have investigated the benefits of power control, with notable examples including [26] and [11]. Specifically, [26] proposes a power allocation strategy for a mono-static sensing scheme in a single-cell ISAC massive MIMO system. In contrast, [11] utilizes distributed radar sensing to estimate the target's location by jointly processing the received signals in a central unit. It also proposes a coordinated power allocation approach where a set of distributed transmitter

¹The acronyms in the table are given as OFDM (orthogonal frequency-division multiplexing), BF (beamforming), SE (spectral efficiency), BER (bit error rate), FD (full-duplex), TX (transmitter), RX (receiver), UL (uplink), DL (downlink), DFRC (dual-functional radar and communications), AF (amplify-and-forward), SINR (signal-to-interference-and-noise ratio), w/w.o (with and without), mMIMO (massive MIMO), SIR (signal-to-interference ratio), V2I (vehicle-to-infrastructure), EKF (extended Kalman filtering), RMSE (root-mean-square error), ESA (effective sensing area), BS (base station), BW (bandwidth), and RL (reinforcement learning).

APs individually serve their corresponding user equipments (UEs) in a cellular-type network. The proposed power allocation approach aims at minimizing the total transmit power while ensuring a minimum signal-to-interference-plus-noise ratio (SINR) for each UE and meeting the required Cramér-Rao lower bound to estimate the location of the target.

To the best of our knowledge, there is limited research on ISAC in cell-free massive MIMO systems. A recent study in [27] provides valuable insights into target detection analysis and the number of required antennas to achieve a certain detection probability. In contrast to our work, this study considers uplink communication and a distributed bi-static sensing scheme with a single transmitter AP. It proposes a protocol using two sensing modes: i) uplink channel estimation and ii) data payload segment of the communication frame. However, the study does not incorporate any power control mechanism. Joint sensing and communication beamforming (BF) design is proposed for a cell-free MIMO system in [28]. The proposed BF design is based on a max-min fairness formulation and is compared with two baseline approaches: i) communication-prioritized sensing BF and ii) sensing-prioritized communication BF. The results in [28] show that the joint design can achieve the communication SINR close to the SINR of the communication-prioritized approach and almost the same sensing SNR achieved by the sensing-prioritized approach. In this work, the authors assume perfect CSI and do not consider the derivation of the target detector. Moreover, the works [27] and [28] neglect the clutter's influence. However, clutter is unavoidable in practical scenarios and acts as interference for sensing which reduces the SINR and degrades the accuracy of target detection. Therefore, further research is necessary to evaluate the performance of ISAC in more practical scenarios.

B. Contributions

Unlike previous works, this paper considers target detection for ISAC in downlink cell-free massive MIMO systems using a multi-static sensing scheme. Two sensing scenarios are analyzed: i) only the downlink communication beams are utilized for sensing; or ii) additional sensing beams with a certain allocated power are jointly transmitted with the communication beams. In the second scenario, we aim to improve the sensing performance by dedicating some resources to sensing.

The communication performance is characterized by the minimum attained SINR by the UEs, and detection probability under a certain false alarm probability is used as the sensing performance metric. False alarm probability is the probability of that the system detects a target when the actual target is not present. A power allocation strategy is developed to optimize the

TABLE I
A LITERATURE OVERVIEW ON ISAC

Category	Ref.	System model	Contributions	Sensing metrics	Communication metrics	Centralization
Mono-static	[15]	OFDM-ISAC	Low-complexity JSAC BF algorithms	Beampattern	SE and BER	—
	[16]	Single-cell narrow-band FD MIMO	Joint TX-RX BF design	TX/RX beampattern, velocity, and range	UL/DL rates	—
	[17]	Cellular DFRC with FDrelay	Joint transceiver design (AF BF design)	Radar SINR, beampattern, and detection probability	Nulling interference from radar	—
	[18]	Single-cell DFRC-MIMO	BF design for three types of communication interference	Mutual information	Rate	—
	[19]	Single-cell with DFRC-MIMO	BF design w/w.o communication interference to radar	Mutual information	Rate	—
	[22]	Single-cell DFRC-MIMO	DFRC BF design under imperfect CSI	Beampattern and detection probability	Achievable data rate	—
	[29]	Multi-antenna FD	An alternative successive interference cancellation scheme	Estimation rate of distance, direction, and velocity	Rate	—
	[26]	Single-cell ISAC mMIMO system	Power allocation to maximize the communication fairness and guarantee a certain radar SIR	Detection probability	Rate	—
	[21]	DFRC V2I	Novel DFRC-based framework and EKF method for vehicle tracking with power allocation and novel predictive BF design	RMSE for angle and distance tracking	Sum rate	—
	[8]	V2I	Predictive BF design	Angle	Sum rate	—
Bi-static	[20]	Cellular	A new JSAC procedure and protocol	ESA, maximum detectable velocity, range, and velocity	BER	—
Distributed bi-static	[27]	Cell-free mMIMO	Protocol for UL communications and distributed bi-static sensing	Detection probability	SE	Fully-centralized
Multi-static	[11]	Multi ISAC-TXs and multi sensing-RXs	Power allocation to minimize the total TX power	Location	SINR	For radar
	[30]	V2I, one vehicle with several BSs	BW allocation and BS selection using RL	Estimation rate	Rate	Central controller
	[31]	Multi-antenna Network ISAC	Coordinated transmit BF	Detection probability	SINR	—
	[28]	Cell-free ISAC MIMO	ISAC BF design	Sensing SNR	SINR	Fully-centralized
	This paper	Cell-free mMIMO	Power allocation to maximize the detection probability while ensuring communication SINR	Detection probability	SINR	Fully-centralized

sensing performance while satisfying SINR constraints for communication UEs, and per-AP transmit power constraints.

To improve sensing performance, we aim to maximize the sensing SINR under the condition that the target is present.² As discussed in [32, Chap. 3 and 15], given a fixed false alarm probability, detection probability increases with a higher signal-to-noise ratio (SNR). The main contributions of this paper are:

- A system model is proposed to consider the joint impact of unknown sensing channel coefficients and clutter. The latter is characterized by the target-free channels between transmitter APs and receiver APs. The channel estimation error is considered for the AP-UE channels, and a new SE expression is obtained by accounting for the interference created

²The optimal design approach would involve optimizing the transmit power coefficients to maximize the probability of detection. However, such an approach poses a significant challenge due to the strong coupling between the test statistics and the power coefficients.

by the additional sensing beams.

- To maximize the sensing SINR while satisfying specific communication SINR constraints, which are equivalent to the SE constraints, a concave-convex programming (CCP)-based power allocation algorithm is proposed. To evaluate the effectiveness of the proposed power allocation algorithm, a communication-centric approach, called *comm.-centric*, is used as the baseline algorithm. The objective of the baseline algorithm is to minimize the total power consumption subject to the same constraints as the proposed algorithm. Conversely, the proposed algorithm maximizes the sensing SINR. Three algorithms are compared numerically: i) the communication-centric (*comm.-centric*); ii) the proposed ISAC power allocation algorithm ii.a) without additional sensing beams (*ISAC*) and ii.b) with dedicated additional sensing beams (*ISAC+S*).
- We derive the maximum a posteriori ratio test (MAPRT) detector for target detection. The detector optimally fuses received signals from the receiver APs during multiple time slots in a centralized manner to detect a target with a known location within a hotspot area. The detector takes into account the presence of clutter, which is not completely canceled out, and the target's unknown radar cross-section (RCS) values. Moreover, we take into account the potential correlation between different arrival and departure directions to/from the target. The new target detector requires more advanced processing compared to the one proposed in our previous work [25], which neglected the existence of clutter. We verify numerically that the proposed advanced processing scheme offers significantly improved detection probability.

The rest of the paper is organized as follows. Section II describes the system model, including the scenario, channel model, and signal model for communication and sensing. Uplink channel estimation and transmit ISAC precoding vectors are presented in Section III, while the downlink communication and SE are provided in Section IV. Sections V and VI are devoted to the multi-static sensing algorithm and deriving the MAPRT detector, respectively. The proposed power allocation algorithm is described in Section VII. The numerical results are discussed in Section VIII. Finally, Section IX concludes the paper.

C. Notations

The following mathematical notations are used throughout the paper. Scalars, vectors, and matrices are denoted by regular font, boldface lowercase, and boldface uppercase letters, respectively. The superscript T shows the transpose operation. Complex conjugate and Hermitian

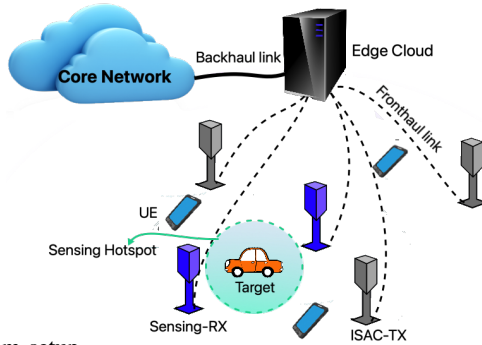


Fig. 1. Illustration of the ISAC system setup.

transpose are illustrated by the superscripts $*$, and H , respectively. The operation of the vectorization of a matrix is represented by $\text{vec}(\cdot)$ and the block diagonalization operation is denoted by $\text{blkdiag}(\cdot)$. The determinant, trace, and real parts of a matrix are represented by $\det(\cdot)$, $\text{Tr}(\cdot)$, and $\Re(\cdot)$, respectively. $\mathbf{A} \otimes \mathbf{B}$ represents the Kronecker product between matrix \mathbf{A} and \mathbf{B} . The absolute value of a scalar is denoted by $|\cdot|$ while $\|\cdot\|$ shows the Euclidean norm of a vector.

II. SYSTEM MODEL

We consider an ISAC system with downlink communication and multi-static sensing in a C-RAN architecture, as illustrated in Fig. 1. In this system, each AP either serves as an ISAC transmitter or a sensing receiver. The number of transmitter and receiver APs are denoted by N_{tx} and N_{rx} at a given instant, respectively. Each AP is equipped with M isotropic antennas deployed as a uniform linear array (ULA).

All APs are connected via fronthaul links to the edge cloud and fully synchronized. We consider the centralized implementation of cell-free massive MIMO [23] for both communication and sensing-related processing. The N_{tx} ISAC transmitter APs jointly serve the N_{ue} UEs by transmitting centrally precoded signals. Optionally, an additional sequence of sensing symbols can be integrated into the transmission that shares the same waveform and time-frequency resources with the communication symbols. When this is the case, the transmitter APs jointly steer a centralized beam toward a potential target with a known location within a hotspot area. On the other hand, the N_{rx} APs operate as sensing receivers by simultaneously sensing the location of the target to determine whether there is a target or not. All processing is done at the edge cloud in a centralized manner.

For simplicity, we assume there is a line-of-sight (LOS) connection between the target location and each transmitter/receiver AP, and the NLOS connections are neglected. Assuming

the antennas at the APs are half-wavelength-spaced, the antenna array response vector for the azimuth angle φ and elevation angle ϑ , denoted by $\mathbf{a}(\varphi, \vartheta) \in \mathbb{C}^M$, is [33]

$$\mathbf{a}(\varphi, \vartheta) = \left[1 \quad e^{j\pi \sin(\varphi) \cos(\vartheta)} \quad \dots \quad e^{j(M-1)\pi \sin(\varphi) \cos(\vartheta)} \right]^T. \quad (1)$$

In this system model, s_i represents the zero-mean downlink communication symbol for UE i with unit power, i.e., $\mathbb{E}\{|s_i|^2\} = 1$. The sensing signal, denoted by s_0 , is also assumed to have zero mean and unit power, i.e., $\mathbb{E}\{|s_0|^2\} = 1$. We assume that the sensing signal is independent of the UEs' data signals to simplify the analysis and power allocation algorithm³. In accordance with [13], the transmitted signal $\mathbf{x}_k[m] \in \mathbb{C}^M$ from transmitter AP k at time instance m can be written as

$$\mathbf{x}_k[m] = \sum_{i=0}^{N_{\text{ue}}} \sqrt{\rho_i} \mathbf{w}_{i,k} s_i[m] = \mathbf{W}_k \mathbf{D}_s[m] \boldsymbol{\rho}, \quad (2)$$

for $k = 1, \dots, N_{\text{tx}}$, where $\mathbf{w}_{i,k} \in \mathbb{C}^M$ and $\mathbf{w}_{0,k} \in \mathbb{C}^M$ are the transmit precoding vectors for transmitter AP k corresponding to UE i and the sensing signal, respectively. In (2), $\mathbf{W}_k = \begin{bmatrix} \mathbf{w}_{0,k} & \mathbf{w}_{1,k} & \dots & \mathbf{w}_{N_{\text{ue}},k} \end{bmatrix}$, $\mathbf{D}_s[m] = \text{diag}(s_0[m], s_1[m], \dots, s_{N_{\text{ue}}}[m])$ is the diagonal matrix containing the sensing and communication symbols, and $\boldsymbol{\rho} = [\sqrt{\rho_0} \quad \dots \quad \sqrt{\rho_{N_{\text{ue}}}}]^T$.

In line with the C-RAN architecture and the centralized operation of cell-free massive MIMO [23], the precoding vectors for each UE and the target are jointly selected based on the CSI from all the $N_{\text{tx}}M$ distributed transmit antennas. Hence, the precoding vectors for each transmitter AP are extracted from the concatenated centralized precoding vectors given as

$$\mathbf{w}_i = \begin{bmatrix} \mathbf{w}_{i,1}^T & \mathbf{w}_{i,2}^T & \dots & \mathbf{w}_{i,N_{\text{tx}}}^T \end{bmatrix}^T \in \mathbb{C}^{N_{\text{tx}}M}, \quad (3)$$

for $i = 0, 1, \dots, N_{\text{ue}}$. As seen in (2), there is a common power control coefficient for each UE, $\rho_i \geq 0$, and for the target, $\rho_0 \geq 0$, since the precoding is centralized. The rationale is to preserve the direction of the centralized precoding vectors in (3) and, hence, not to destroy its favorable characteristics constructed based on the overall channel from $N_{\text{tx}}M$ antennas. Using the independence of the data and sensing signals, the average transmit power for transmitter AP k is given as

$$P_k = \mathbb{E} \{ \|\mathbf{x}_k[m]\|^2 \} = \sum_{i=0}^{N_{\text{ue}}} \rho_i \mathbb{E} \{ \|\mathbf{w}_{i,k}\|^2 \}, \quad k = 1, \dots, N_{\text{tx}}. \quad (4)$$

Each of the average transmit powers should satisfy the maximum power limit P_{tx} , i.e., $P_k \leq P_{\text{tx}}$.

We consider block fading communication channels where we have constant and independent channel realizations in each time-frequency coherence block. We let $\mathbf{h}_{i,k} \in \mathbb{C}^M$ denote the

³The sensing signal can instead be selected as a linear combination of UEs' data signals to potentially improve the communication performance for the UEs nearby the hotspot area. We leave the analysis for this case to future work.

channel from transmitter AP k to UE i . We assume a correlated Rayleigh fading distribution for which $\mathbf{h}_{i,k} \sim \mathcal{CN}(\mathbf{0}, \mathbf{R}_{i,k})$ where $\mathbf{R}_{i,k} = \mathbb{E} \{ \mathbf{h}_{i,k} \mathbf{h}_{i,k}^H \}$ is the spatial correlation matrix that includes the combined effect of geometric path loss, shadowing, and spatial correlation among the antennas for the channel realizations. We define the communication channel from all the $N_{\text{tx}}M$ transmit antennas to UE i in the network as $\mathbf{h}_i = \left[\mathbf{h}_{i,1}^T \ \dots \ \mathbf{h}_{i,N_{\text{tx}}}^T \right]^T \in \mathbb{C}^{N_{\text{tx}}M}$. Similarly, the concatenated array response vector from all the $N_{\text{tx}}M$ transmit antennas to the target is given by $\mathbf{h}_0 = \left[\mathbf{a}^T(\varphi_1, \vartheta_1) \ \dots \ \mathbf{a}^T(\varphi_{N_{\text{tx}}}, \vartheta_{N_{\text{tx}}}) \right]^T \in \mathbb{C}^{N_{\text{tx}}M}$ using (1). Here, φ_k and ϑ_k are the azimuth and elevation angles from transmitter AP k to the target location, respectively.

Imperfect CSI of communication channels is considered, and the minimum mean-squared error (MMSE) channel estimation approach is used during the uplink channel estimation phase.

III. UPLINK CHANNEL ESTIMATION AND TRANSMIT ISAC PRECODING VECTORS

In this section, we will explicate the channel estimation procedure that leverages the transmitted uplink pilot symbols and elaborate on the selection of the ISAC precoding vectors based on the estimated UE channels and the location of the sensing point.

A. Uplink Channel Estimation

Let us define the length of the coherence blocks and the pilot sequences by τ_c and $\tau_p < \tau_c$, respectively. Moreover, a set of τ_p mutually orthogonal pilot sequences are denoted by $\phi_1, \dots, \phi_{\tau_p} \in \mathbb{C}^{\tau_p}$, where $\|\phi_t\|^2 = \tau_p$, for $t = 1, \dots, \tau_p$. The pilot sequences are assigned to the N_{ue} UEs. If the number of pilot sequences is less than the number of UEs (i.e., $\tau_p < N_{\text{ue}}$), then each pilot sequence may be assigned to multiple UEs. Let $t_i \in \{1, \dots, \tau_p\}$ denote the index of the pilot sequence that is assigned to UE i , and we define $\mathcal{P}_i = \{j \in \{1, \dots, N_{\text{ue}}\} | t_j = t_i\}$ as the set of UEs that share the same pilot with UE i including itself. The received signal at the ISAC transmitter AP k during the entire pilot transmission is denoted by $\mathbf{Y}_k^p \in \mathbb{C}^{M \times \tau_p}$ where

$$\mathbf{Y}_k^p = \sum_{i=1}^{N_{\text{ue}}} \sqrt{\eta_i} \mathbf{h}_{i,k} \phi_{t_i}^T + \mathbf{N}_k, \quad (5)$$

where $\eta_i > 0$ is the transmit power by UE i and $\mathbf{N}_k \in \mathbb{C}^{M \times \tau_p}$ is the received noise at AP k with independent and identically distributed (i.i.d.) $\mathcal{CN}(0, \sigma_n^2)$ entries. We employ the standard MMSE channel estimator [23]. With respect to estimating $\mathbf{h}_{i,k}$, we form $\mathbf{y}_{t_i,k}^p = \frac{1}{\sqrt{\tau_p}} \mathbf{Y}_k^p \phi_{t_i}^* \in \mathbb{C}^M$ as

$$\mathbf{y}_{t_i,k}^p = \underbrace{\sqrt{\eta_i \tau_p} \mathbf{h}_{i,k}}_{\text{Desired part}} + \underbrace{\sum_{j \in \mathcal{P}_i \setminus \{i\}} \sqrt{\eta_j \tau_p} \mathbf{h}_{j,k}}_{\text{Interference part}} + \underbrace{\mathbf{n}_{t_i,k}}_{\text{Noise}}, \quad (6)$$

where $\mathbf{n}_{t_i,k} = \frac{1}{\sqrt{\tau_p}} \mathbf{N}_k \phi_{t_i}^* \sim \mathcal{CN}(\mathbf{0}, \sigma_n^2 \mathbf{I}_M)$. By [23, Cor. 4.1], the MMSE estimate of $\mathbf{h}_{i,k}$ is

$$\hat{\mathbf{h}}_{i,k} = \sqrt{\eta_i \tau_p} \mathbf{R}_{i,k} \Psi_{t_i,k}^{-1} \mathbf{y}_{t_i,k}^p, \quad (7)$$

where $\mathbf{R}_{i,k}$ and $\Psi_{t_i,k}$ are the spatial correlation matrix corresponding to channel $\mathbf{h}_{i,k}$ and the correlation matrix of the received signal, respectively, is given by

$$\mathbf{R}_{i,k} = \mathbb{E} \{ \mathbf{h}_{i,k} \mathbf{h}_{i,k}^H \}, \quad \Psi_{t_i,k} = \mathbb{E} \left\{ \mathbf{y}_{t_i,k}^p (\mathbf{y}_{t_i,k}^p)^H \right\} = \sum_{j \in \mathcal{P}_i} \eta_j \tau_p \mathbf{R}_{j,k} + \sigma_n^2 \mathbf{I}_M. \quad (8)$$

The channel estimation error is $\tilde{\mathbf{h}}_{i,k} = \mathbf{h}_{i,k} - \hat{\mathbf{h}}_{i,k}$ where $\tilde{\mathbf{h}}_{i,k} \sim \mathcal{CN}(\mathbf{0}, \mathbf{C}_{i,k})$ and the error correlation matrix is

$$\mathbf{C}_{i,k} = \mathbb{E} \left\{ \tilde{\mathbf{h}}_{i,k} \tilde{\mathbf{h}}_{i,k}^H \right\} = \mathbf{R}_{i,k} - \eta_i \tau_p \mathbf{R}_{i,k} \Psi_{t_i,k}^{-1} \mathbf{R}_{i,k}. \quad (9)$$

B. Transmit ISAC Precoding Vectors

The unit-norm regularized zero-forcing (RZF) precoding vector [23] is constructed for UE i as $\mathbf{w}_i = \frac{\bar{\mathbf{w}}_i}{\|\bar{\mathbf{w}}_i\|}$, where

$$\bar{\mathbf{w}}_i = \left(\sum_{j=1}^{N_{\text{ue}}} \hat{\mathbf{h}}_j \hat{\mathbf{h}}_j^H + \lambda \mathbf{I}_{N_{\text{tx}}M} \right)^{-1} \hat{\mathbf{h}}_i, \quad i = 1, \dots, N_{\text{ue}}, \quad (10)$$

and λ is the regularization parameter. Note that since the communication symbols also contribute to sensing by the reflected paths toward the target, they are not considered as interference for the sensing target. Hence, we aim at nulling the interference only for the UEs. To null the destructive interference from the sensing signal to the UEs, the sensing precoding vector \mathbf{w}_0 can be selected as the ZF precoder, i.e., by projecting \mathbf{h}_0 onto the nullspace of the subspace spanned by the UE channel vectors as in [13], i.e.,

$$\mathbf{w}_0 = \frac{(\mathbf{I}_{N_{\text{tx}}M} - \mathbf{U}\mathbf{U}^H) \mathbf{h}_0}{\|(\mathbf{I}_{N_{\text{tx}}M} - \mathbf{U}\mathbf{U}^H) \mathbf{h}_0\|}, \quad (11)$$

where \mathbf{U} is the unitary matrix with the orthogonal columns that span the column space of the matrix $\begin{bmatrix} \hat{\mathbf{h}}_1 & \dots & \hat{\mathbf{h}}_{N_{\text{ue}}} \end{bmatrix}$.

IV. DOWNLINK COMMUNICATION AND SPECTRAL EFFICIENCY FOR ISAC

The received signal at UE i is given as

$$\begin{aligned} y_i[m] &= \sum_{k=1}^{N_{\text{tx}}} \mathbf{h}_{i,k}^H \mathbf{x}_k[m] + n_i[m] = \underbrace{\sqrt{\rho_i} \mathbf{h}_i^H \mathbf{w}_i s_i[m]}_{\text{Desired signal}} \\ &+ \underbrace{\sum_{j=1, j \neq i}^{N_{\text{ue}}} \sqrt{\rho_j} \mathbf{h}_i^H \mathbf{w}_j s_j[m]}_{\text{Interference signal due to the other UEs}} + \underbrace{\sqrt{\rho_0} \mathbf{h}_i^H \mathbf{w}_0 s_0[m]}_{\text{Interference signal due to the sensing}} + \underbrace{n_i[m]}_{\text{Noise}}, \quad (12) \end{aligned}$$

where the receiver noise at the UE i is represented by $n_i[m] \sim \mathcal{CN}(0, \sigma_n^2)$. We introduce the complex conjugation on the channels $\mathbf{h}_{i,k}$ for notational convenience in the downlink, as it is

defined in [25]. The following lemma presents an achievable SE for each UE i , for $i = 1, \dots, N_{\text{ue}}$.

Lemma 1. *For a C-RAN-assisted cell-free massive MIMO system with ISAC, where only $\mathbb{E}\{\mathbf{h}_i^H \mathbf{w}_i\}$ is known at UE i , an achievable SE of this UE is given by*

$$\text{SE}_i^{(\text{dl})} = \frac{\tau_c - \tau_p}{\tau_c} \log_2 \left(1 + \text{SINR}_i^{(\text{dl})} \right), \quad (13)$$

with

$$\text{SINR}_i^{(\text{dl})} = \frac{\rho_i |\mathbb{E}\{\mathbf{h}_i^H \mathbf{w}_i\}|^2}{\sum_{j=1}^{N_{\text{ue}}} \rho_j \mathbb{E}\{|\mathbf{h}_i^H \mathbf{w}_j|^2\} - \rho_i |\mathbb{E}\{\mathbf{h}_i^H \mathbf{w}_i\}|^2 + \rho_0 \mathbb{E}\{|\tilde{\mathbf{h}}_i^H \mathbf{w}_0|^2\} + \sigma_n^2}, \quad (14)$$

where $\tilde{\mathbf{h}}_i = [\tilde{\mathbf{h}}_{i,1}^T \ \dots \ \tilde{\mathbf{h}}_{i,N_{\text{tx}}}^T]^T \in \mathbb{C}^{N_{\text{tx}}M}$ is the concatenated channel estimation error.

Proof. See Appendix A. □

The first two terms in the denominator of (14) is related to the interference power due to the other UEs in the system and self interference, while the third one, i.e., $\rho_0 \mathbb{E}\{|\tilde{\mathbf{h}}_i^H \mathbf{w}_0|^2\}$ is the interference power coming from the sensing symbols. The pre-log factor represents the fraction of the downlink data within a coherence block.

The SE given above is achievable when channel coding is applied over a long data sequence during many coherence blocks. In line with this requirement, we assume that we have multiple target locations in the system where sensing each of them takes a portion of the whole communication interval. This implies that the precoding vector \mathbf{w}_0 changes over time during the whole communication interval according to different locations of the targets and the channels of UEs that vary from coherence block to coherence block. Therefore, the expectation $\mathbb{E}\{|\tilde{\mathbf{h}}_i^H \mathbf{w}_0|^2\}$ in (14) should be taken over both \mathbf{h}_i and \mathbf{w}_0 for different channel realizations and sensing locations. This can be done using Monte Carlo simulation.

V. MULTI-STATIC SENSING

We consider multi-static sensing where the sensing transmitters and the receivers are not co-located. Apart from the N_{tx} transmitter APs, the other N_{rx} receiver APs jointly receive the sensing signals for target detection. Each receiver AP receives both desired and undesired signals when the target is present. The former is the reflected signals from the target, while the latter is independent of the presence of the target.

Apart from the noise, the undesired signal includes clutter and LOS paths between transmitter and receiver APs. Clutter is composed of two terms: i) the non-line-of-sight (NLOS) paths due to scattering/reflection by the permanent objects and ii) the NLOS paths due to the temporary obstacles in the environment. The location and shape of permanent objects such as buildings, walls, or mountains are typically fixed and can be modeled accurately. This means that the LOS and NLOS paths caused by these permanent obstacles can be estimated or measured beforehand using various techniques such as ray tracing, simulation, or empirical models. Therefore, we assume that the LOS and NLOS paths due to the permanent obstacles are known. Assuming the transmit signal $\mathbf{x}_k[m]$ is also known at the edge cloud, the known undesired parts of the received signal at each receiver AP can be canceled. However, the unknown part corresponding to the NLOS paths caused by temporary obstacles remains.

Let us denote the unknown NLOS channel matrix between transmitter AP k and receiver AP r by $\mathbf{H}_{r,k} \in \mathbb{C}^{M \times M}$. These channels correspond to the reflected paths through the temporary obstacles and are henceforth referred to as target-free channels. After canceling the known undesired terms, the received signal at AP r in the presence of the target is formulated as

$$\mathbf{y}_r[m] = \sum_{k=1}^{N_{\text{tx}}} \alpha_{r,k} \underbrace{\sqrt{\beta_{r,k}} \mathbf{a}(\phi_r, \theta_r) \mathbf{a}^T(\varphi_k, \vartheta_k) \mathbf{x}_k[m]}_{\triangleq \mathbf{g}_{r,k}[m]} + \sum_{k=1}^{N_{\text{tx}}} \underbrace{\mathbf{H}_{r,k} \mathbf{x}_k[m]}_{\text{Interference}} + \mathbf{n}_r[m]. \quad (15)$$

where $\mathbf{n}_r[m] \sim \mathcal{CN}(\mathbf{0}, \sigma_n^2 \mathbf{I}_M)$ is the receiver noise at the M antennas of receiver AP r . The defined vector $\mathbf{g}_{r,k}[m] \in \mathbb{C}^M$ in (15) is the known part of each reflected path. The vector $\mathbf{H}_{r,k} \mathbf{x}_k[m]$ can be considered as the interference for the target detection. The matrix $\alpha_{r,k} \sqrt{\beta_{r,k}} \mathbf{a}(\phi_r, \theta_r) \mathbf{a}^T(\varphi_k, \vartheta_k)$ represents the reflected path through the target where ϕ_r and θ_r are respectively the azimuth and elevation angles from the target location to receiver AP r . Here, $\alpha_{r,k}$ is the bi-static unknown RCS of the target through the reflection path from transmitter AP k to receiver AP r . We follow the Swerling-I model for the RCS, in which the target's velocity is low compared to the total sensing duration. Hence, $\alpha_{r,k}$ is constant throughout the consecutive symbols collected for sensing according to the distribution $\alpha_{r,k} \sim \mathcal{CN}(0, \sigma_{r,k}^2)$. The $\beta_{r,k}$ is the channel gain of the path from transmitter AP k to the target and then from the target to the receiver AP r . We inject the phase-shift of this path to the unknown complex-valued RCS $\alpha_{r,k}$ without loss of generality.

Let us define $d_{\text{tx},k}$ as the distance between transmitter AP k and target location and $d_{\text{rx},r}$ as the distance between receiver AP r and target location. Using the radar range equation for bi-static

sensing in [32, Chap. 2], the channel gain $\beta_{r,k}$ can be computed as

$$\beta_{r,k} = \frac{\lambda_c^2}{(4\pi)^3 d_{\text{tx},k}^2 d_{\text{rx},r}^2}, \quad (16)$$

where λ_c is the carrier wavelength.

Each receiver AP sends their respective signals $\mathbf{y}_r[m]$, for $r = 1, \dots, N_{\text{rx}}$, to the edge cloud. The received signals from all the N_{rx} APs can be concatenated to obtain the overall sensing signal

$$\mathbf{y}[m] = \left[\mathbf{y}_1^T[m] \ \dots \ \mathbf{y}_{N_{\text{rx}}}^T[m] \right]^T \in \mathbb{C}^{N_{\text{rx}}M}. \quad (17)$$

We use the correlated Rayleigh fading model for the NLOS channels $\mathbf{H}_{r,k}$, which is modeled using the Kronecker model [34]. Let us define the random matrix $\mathbf{W}_{\text{ch},(r,k)} \in \mathbb{C}^{M \times M}$ with i.i.d. entries with $\mathcal{CN}(0, 1)$ distribution. The matrix $\mathbf{R}_{\text{rx},(r,k)} \in \mathbb{C}^{M \times M}$ represents the spatial correlation matrix corresponding to receiver AP r and with respect to the direction of transmitter AP k . Similarly, $\mathbf{R}_{\text{tx},(r,k)} \in \mathbb{C}^{M \times M}$ is the spatial correlation matrix corresponding to transmitter AP k and with respect to the direction of receiver AP r . Then, the channel $\mathbf{H}_{r,k}$ is written as

$$\mathbf{H}_{r,k} = \mathbf{R}_{\text{rx},(r,k)}^{\frac{1}{2}} \mathbf{W}_{\text{ch},(r,k)} \left(\mathbf{R}_{\text{tx},(r,k)}^{\frac{1}{2}} \right)^T, \quad (18)$$

where the channel gain is determined by the geometric path loss and shadowing, and is included in the spatial correlation matrices. Now, we define $\mathbf{h}_{r,k} = \text{vec}(\mathbf{H}_{r,k})$ as the vectorized unknown target-free channel between receiver AP r and the transmitter AP k where $\mathbf{h}_{r,k} \sim \mathcal{CN}(\mathbf{0}, \bar{\mathbf{R}}_{r,k}) \in \mathbb{C}^{M^2}$. Then, the channel vector $\mathbf{h}_{r,k}$ can be expressed as

$$\mathbf{h}_{r,k} = \underbrace{\left(\mathbf{R}_{\text{tx},(r,k)}^{\frac{1}{2}} \otimes \mathbf{R}_{\text{rx},(r,k)}^{\frac{1}{2}} \right)}_{=\bar{\mathbf{R}}_{r,k}^{\frac{1}{2}}} \text{vec}(\mathbf{W}_{\text{ch},(r,k)}), \quad (19)$$

where we have used the identity $\text{vec}(\mathbf{ABC}) = (\mathbf{C}^T \otimes \mathbf{A})\text{vec}(\mathbf{B})$ with $\mathbf{A} = \mathbf{R}_{\text{rx},(r,k)}^{\frac{1}{2}}$, $\mathbf{B} = \mathbf{W}_{\text{ch},(r,k)}$, and $\mathbf{C} = \mathbf{R}_{\text{tx},(r,k)}^{\frac{1}{2}}$. We also recognize the square root of the spatial correlation matrix $\bar{\mathbf{R}}_{r,k}$ by noting that $\mathbb{E} \left\{ \text{vec}(\mathbf{W}_{\text{ch},(r,k)}) \text{vec}(\mathbf{W}_{\text{ch},(r,k)})^H \right\} = \mathbf{I}_{M^2}$. Similarly, the interference signal for each receiver AP r can be rewritten as

$$\sum_{k=1}^{N_{\text{tx}}} \mathbf{H}_{r,k} \mathbf{x}_k[m] = \sum_{k=1}^{N_{\text{tx}}} (\mathbf{x}_k^T[m] \otimes \mathbf{I}_M) \mathbf{h}_{r,k} = (\mathbf{x}^T[m] \otimes \mathbf{I}_M) \mathbf{h}_r, \quad (20)$$

where we concatenate the unknown and known parts of the interference signals, respectively as

$$\mathbf{h}_r = \left[\mathbf{h}_{r,1}^T \ \dots \ \mathbf{h}_{r,N_{\text{tx}}}^T \right]^T \in \mathbb{C}^{N_{\text{tx}}M^2}, \quad \mathbf{x}[m] = \left[\mathbf{x}_1^T[m] \ \dots \ \mathbf{x}_{N_{\text{tx}}}^T[m] \right]^T \in \mathbb{C}^{N_{\text{tx}}M}. \quad (21)$$

To introduce a more concise notation, we concatenate the unknown sensing channel coefficients for each receiver r as $\boldsymbol{\alpha}_r \triangleq [\alpha_{r,1} \ \dots \ \alpha_{r,N_{\text{tx}}}]^T \in \mathbb{C}^{N_{\text{tx}}}$, then collect all $\boldsymbol{\alpha}_r$ terms in a vector as

$\boldsymbol{\alpha} = [\boldsymbol{\alpha}_1^T \dots \boldsymbol{\alpha}_{N_{\text{rx}}}^T]^T \in \mathbb{C}^{N_{\text{tx}}N_{\text{rx}}}$. Moreover, using $\mathbf{g}_{r,k}[m]$ from (15), which is the known part of the received sensing signal, we define the concatenated matrix for receiver AP r and symbol m as $\mathbf{G}_r[m] = [\mathbf{g}_{r,1}[m] \dots \mathbf{g}_{r,N_{\text{tx}}}[m]] \in \mathbb{C}^{M \times N_{\text{tx}}}$. Then, the overall received signal in (17) can be expressed as

$$\mathbf{y}[m] = \underbrace{\text{blkdiag}(\mathbf{G}_1[m], \dots, \mathbf{G}_{N_{\text{rx}}}[m])}_{\triangleq \mathbf{G}[m]} \boldsymbol{\alpha} + \underbrace{(\mathbf{I}_{N_{\text{rx}}} \otimes (\mathbf{x}^T[m] \otimes \mathbf{I}_M))}_{\triangleq \mathbf{X}[m]} \mathbf{h} + \mathbf{n}[m], \quad (22)$$

where $\text{blkdiag}(\cdot)$ constructs a block diagonal matrix, $\mathbf{h} = [\mathbf{h}_1^T \dots \mathbf{h}_{N_{\text{rx}}}^T]^T \in \mathbb{C}^{N_{\text{tx}}N_{\text{rx}}M^2}$, and $\mathbf{n}[m] = [\mathbf{n}_1^T[m] \dots \mathbf{n}_{N_{\text{rx}}}^T[m]]^T \in \mathbb{C}^{N_{\text{rx}}M}$ is the concatenated receiver noise. Given that the channels $\mathbf{H}_{r,k}$ are independent for different r and/or k (due to sufficiently separated APs), the correlation matrix of \mathbf{h} becomes the block diagonal matrix of the spatial correlation matrices $\overline{\mathbf{R}}_{r,k}$, i.e.,

$$\mathbf{R} = \mathbb{E} \{ \mathbf{h} \mathbf{h}^H \} = \text{blkdiag}(\overline{\mathbf{R}}_{1,1}, \dots, \overline{\mathbf{R}}_{1,N_{\text{tx}}}, \dots, \overline{\mathbf{R}}_{N_{\text{rx}},1}, \dots, \overline{\mathbf{R}}_{N_{\text{rx}},N_{\text{tx}}}). \quad (23)$$

VI. MAPRT DETECTOR FOR SENSING

In this paper, the detection probability, denoted by P_d , is utilized to evaluate the sensing performance. P_d is defined as the probability of detecting the target given that it is present. We employ the MAPRT detector for our system model and extend the derivation in [35], which considers only a single transmitter and single-antenna receivers.

Different from [35], in our system, the transmitted signals are known due to the C-RAN architecture. Furthermore, the relationship between the received signals at the receiver APs and the unknown RCSs is more complex due to the direction-dependent MIMO channels from the transmitter APs to the receiver APs through the target. Our derived test statistics demonstrates not only how the detector should be implemented but also how the different signals from the receiver APs should be centrally fused in the edge cloud. The detection is applied using τ received sensing symbols for a particular target location. Let us define the vectors $\mathbf{y}_\tau \in \mathbb{C}^{MN_{\text{rx}}\tau}$, $\mathbf{n}_\tau \in \mathbb{C}^{MN_{\text{rx}}\tau}$, $\mathbf{h}_\tau \in \mathbb{C}^{MN_{\text{rx}}\tau}$, and $\mathbf{g}_\tau \in \mathbb{C}^{MN_{\text{rx}}\tau}$ constructed by concatenating $\mathbf{y}[m]$, $\mathbf{n}[m]$, $\mathbf{X}[m]\mathbf{h}$, and $\mathbf{G}[m]\boldsymbol{\alpha}$ in (22), respectively for τ symbols. The binary hypothesis used in the MAPRT detector is written as

$$\begin{aligned} \mathcal{H}_0 : \mathbf{y}_\tau &= \mathbf{h}_\tau + \mathbf{n}_\tau \\ \mathcal{H}_1 : \mathbf{y}_\tau &= \mathbf{g}_\tau + \mathbf{h}_\tau + \mathbf{n}_\tau. \end{aligned} \quad (24)$$

The null hypothesis \mathcal{H}_0 represents the case that there is no target in the sensing area, while the alternative hypothesis \mathcal{H}_1 represents the existence of the target. We let $\mathcal{H} \in \{\mathcal{H}_0, \mathcal{H}_1\}$ be the

set of hypotheses. We also recall that $\boldsymbol{\alpha}$ and \mathbf{h} are the vector of unknown channel gains with respect to the RCS of the target and the vector of unknown channel gains with respect to the target-free channels, respectively. The joint RCS estimation, target-free channel estimation, and hypothesis testing problem can be written as

$$\left(\hat{\boldsymbol{\alpha}}, \hat{\mathbf{h}}, \hat{\mathcal{H}}\right) = \arg \max_{\boldsymbol{\alpha}, \mathbf{h}, \mathcal{H}} p(\boldsymbol{\alpha}, \mathbf{h}, \mathcal{H} | \mathbf{y}_\tau), \quad (25)$$

where $p(\boldsymbol{\alpha}, \mathbf{h}, \mathcal{H} | \mathbf{y}_\tau)$ is the joint probability density function of $\boldsymbol{\alpha}$, \mathbf{h} , and \mathcal{H} given the received signal vector \mathbf{y}_τ . Following the approach in [35] and [25] for our problem and assuming $\boldsymbol{\alpha}$ and \mathbf{h} are independent of each other, the corresponding MAPRT detector can be expressed as

$$\Lambda = \frac{\max_{\boldsymbol{\alpha}, \mathbf{h}} p(\mathbf{y}_\tau | \boldsymbol{\alpha}, \mathbf{h}, \mathcal{H}_1) p(\boldsymbol{\alpha} | \mathcal{H}_1) p(\mathbf{h} | \mathcal{H}_1)}{\max_{\mathbf{h}} p(\mathbf{y}_\tau | \mathbf{h}, \mathcal{H}_0) p(\mathbf{h} | \mathcal{H}_0)} \underset{\mathcal{H}_0}{\overset{\mathcal{H}_1}{\geq}} \lambda_d, \quad (26)$$

where λ_d is the threshold used by the detector, which is selected to achieve a desired false alarm probability and $p(\cdot)$ denotes the probability density function (PDF). In (26), we maximize the joint PDFs with respect to the estimation parameters in (25) under the hypothesis \mathcal{H}_1 and \mathcal{H}_0 in the numerator and the denominator, respectively. To streamline the analysis, we define the above-mentioned optimization problems by Λ_{num} and Λ_{den} , respectively, which are expressed as

$$\Lambda_{\text{num}} = \max_{\boldsymbol{\alpha}, \mathbf{h}} p(\mathbf{y}_\tau | \boldsymbol{\alpha}, \mathbf{h}, \mathcal{H}_1) p(\boldsymbol{\alpha} | \mathcal{H}_1) p(\mathbf{h} | \mathcal{H}_1), \quad (27)$$

$$\Lambda_{\text{den}} = \max_{\mathbf{h}} p(\mathbf{y}_\tau | \mathbf{h}, \mathcal{H}_0) p(\mathbf{h} | \mathcal{H}_0). \quad (28)$$

The solutions to these optimization problems under \mathcal{H}_0 and \mathcal{H}_1 are presented in Lemma 2.

Lemma 2. *Consider the binary hypothesis defined in (24) and the overall received signal for sensing for all time instants $m \in \{1, \dots, \tau\}$ as defined in (22). Given that $\mathbf{h} \sim \mathcal{CN}(\mathbf{0}, \mathbf{R})$ and $\boldsymbol{\alpha} \sim \mathcal{CN}(\mathbf{0}, \mathbf{R}_{\text{rcs}})$, where \mathbf{R}_{rcs} is the covariance matrix of the correlated RCS values, we have the following results.*

Optimization under \mathcal{H}_0 : *Given that the hypothesis \mathcal{H}_0 is true, the denominator of the likelihood ratio in (26) is*

$$\Lambda_{\text{den}} = C_1 C_2 \exp\left(\frac{\mathbf{b}^H \mathbf{D}^{-1} \mathbf{b} - F}{\sigma_n^2}\right), \quad (29)$$

where $C_1 = \frac{1}{(\pi \sigma_n^2)^{M N_{\text{rx}} \tau}}$ and $C_2 = \frac{1}{\pi^{M^2 N_{\text{tx}} N_{\text{rx}}} \det(\mathbf{R})}$. The matrix \mathbf{D} , the vector \mathbf{b} , and the scalar F are defined in (32), (31), and (33), respectively.

Optimization under \mathcal{H}_1 : Given that the hypothesis \mathcal{H}_1 is true, the numerator of the likelihood ratio in (26) is given as

$$\Lambda_{\text{num}} = C_1 C_2 C_3 \exp \left(\frac{1}{\sigma_n^2} \begin{bmatrix} \mathbf{a}^H & \mathbf{b}^H \end{bmatrix} \begin{bmatrix} \mathbf{C} & \mathbf{E} \\ \mathbf{E}^H & \mathbf{D} \end{bmatrix}^{-1} \begin{bmatrix} \mathbf{a} \\ \mathbf{b} \end{bmatrix} - \frac{1}{\sigma_n^2} F \right), \quad (30)$$

where

$$\mathbf{a} = \sum_{m=1}^{\tau} \mathbf{G}^H[m] \mathbf{y}[m], \quad \mathbf{b} = \sum_{m=1}^{\tau} \mathbf{X}^H[m] \mathbf{y}[m], \quad (31)$$

$$\mathbf{C} = \sum_{m=1}^{\tau} \mathbf{G}^H[m] \mathbf{G}[m] + \sigma_n^2 \mathbf{R}_{\text{rcs}}^{-1}, \quad \mathbf{D} = \sum_{m=1}^{\tau} \mathbf{X}^H[m] \mathbf{X}[m] + \sigma_n^2 \mathbf{R}^{-1}, \quad (32)$$

$$\mathbf{E} = \sum_{m=1}^{\tau} \mathbf{G}^H[m] \mathbf{X}[m], \quad F = \sum_{m=1}^{\tau} \|\mathbf{y}[m]\|^2. \quad (33)$$

Proof. See Appendix B. □

By substituting (29) and (30) into (26), the MAPRT detector is obtained as

$$\Lambda = C_3 \exp \left(\frac{1}{\sigma_n^2} \begin{bmatrix} \mathbf{a}^H & \mathbf{b}^H \end{bmatrix} \left(\begin{bmatrix} \mathbf{C} & \mathbf{E} \\ \mathbf{E}^H & \mathbf{D} \end{bmatrix}^{-1} - \begin{bmatrix} \mathbf{0} & \mathbf{0} \\ \mathbf{0} & \mathbf{D}^{-1} \end{bmatrix} \right) \begin{bmatrix} \mathbf{a} \\ \mathbf{b} \end{bmatrix} \right) \underset{\mathcal{H}_0}{\overset{\mathcal{H}_1}{\geq}} \lambda_d. \quad (34)$$

Now, let us define the test statistics $T \triangleq \ln(\Lambda)$, which is given as

$$T = \ln(C_3) + \frac{1}{\sigma_n^2} \left(\begin{bmatrix} \mathbf{a}^H & \mathbf{b}^H \end{bmatrix} \left(\begin{bmatrix} \mathbf{C} & \mathbf{E} \\ \mathbf{E}^H & \mathbf{D} \end{bmatrix}^{-1} - \begin{bmatrix} \mathbf{0} & \mathbf{0} \\ \mathbf{0} & \mathbf{D}^{-1} \end{bmatrix} \right) \begin{bmatrix} \mathbf{a} \\ \mathbf{b} \end{bmatrix} \right). \quad (35)$$

Finally, the decision is taken as follows

$$\hat{\mathcal{H}} = \begin{cases} \mathcal{H}_1 & \text{if } T \geq \ln(\lambda_d), \\ \mathcal{H}_0 & \text{if } T < \ln(\lambda_d). \end{cases} \quad (36)$$

VII. POWER ALLOCATION FOR ISAC

In Section VI, we have derived the MAPRT detector. It uses the already selected power allocation strategy, which is the second stage of our two-stage design approach. In this section, we maximize the sensing SINR, denoted by SINR_s , under the presumption that the target is present. The optimization problem can be cast as

$$\underset{\boldsymbol{\rho} \geq \mathbf{0}}{\text{maximize}} \quad \text{SINR}_s \quad (37a)$$

$$\text{subject to} \quad \text{SINR}_i^{(\text{dl})} \geq \gamma_c, \quad i = 1, \dots, N_{\text{ue}} \quad (37b)$$

$$P_k \leq P_{\text{tx}}, \quad k = 1, \dots, N_{\text{tx}} \quad (37c)$$

where γ_c is the minimum required SINR threshold to provide a certain SE to all the UEs and P_{tx} is the maximum transmit power per AP. The sensing SINR is given as

$$\text{SINR}_s = \frac{\boldsymbol{\rho}^T \mathbf{A} \boldsymbol{\rho}}{\tau M N_{\text{rx}} \sigma_n^2 + \boldsymbol{\rho}^T \mathbf{B} \boldsymbol{\rho}}, \quad (38)$$

where

$$\begin{aligned} \mathbf{A} = & \sum_{m=1}^{\tau} \mathbf{D}_s^H[m] \left(\sum_{r=1}^{N_{\text{rx}}} \sum_{k=1}^{N_{\text{tx}}} \sum_{j=1}^{N_{\text{tx}}} \sqrt{\beta_{r,k} \beta_{r,j}} \mathbf{W}_k^H \mathbf{a}^*(\varphi_k, \vartheta_k) \mathbf{a}^H(\phi_r, \theta_r) \right. \\ & \left. \times \text{cov}(\alpha_{r,j}, \alpha_{r,k}) \mathbf{a}(\phi_r, \theta_r) \mathbf{a}^T(\varphi_j, \vartheta_j) \mathbf{W}_j \right) \mathbf{D}_s[m], \end{aligned} \quad (39)$$

and

$$\mathbf{B} = \sum_{m=1}^{\tau} \mathbf{D}_s^H[m] \left(\sum_{r=1}^{N_{\text{rx}}} \sum_{k=1}^{N_{\text{tx}}} \text{tr}(\mathbf{R}_{\text{rx},(r,k)}) \mathbf{W}_k^H \mathbf{R}_{\text{tx},(r,k)}^T \mathbf{W}_k \right) \mathbf{D}_s[m]. \quad (40)$$

The derivation of (38) is given in Appendix C. The matrices \mathbf{A} and \mathbf{B} are Hermitian symmetric. Since the entries of $\boldsymbol{\rho}$ are real valued, we have $\boldsymbol{\rho}^T \mathbf{A} \boldsymbol{\rho} = \boldsymbol{\rho}^T \Re(\mathbf{A}) \boldsymbol{\rho}$ and $\boldsymbol{\rho}^T \mathbf{B} \boldsymbol{\rho} = \boldsymbol{\rho}^T \Re(\mathbf{B}) \boldsymbol{\rho}$. Let us define $\mathbf{A}_r = \Re(\mathbf{A})$ and $\mathbf{B}_r = \Re(\mathbf{B})$. Then, the sensing SINR can be written as

$$\text{SINR}_s = \frac{\boldsymbol{\rho}^T \mathbf{A}_r \boldsymbol{\rho}}{\tau M N_{\text{rx}} \sigma_n^2 + \boldsymbol{\rho}^T \mathbf{B}_r \boldsymbol{\rho}}. \quad (41)$$

It can be shown that the optimization problem in (37) is equivalent to [36]

$$\underset{\boldsymbol{\rho} \geq \mathbf{0}, t}{\text{maximize}} \quad \frac{\boldsymbol{\rho}^T \mathbf{A}_r \boldsymbol{\rho}}{t} \quad (42a)$$

$$\text{subject to} \quad \tau M N_{\text{rx}} \sigma_n^2 + \boldsymbol{\rho}^T \mathbf{B}_r \boldsymbol{\rho} \leq t \quad (42b)$$

$$\text{SINR}_i^{(\text{dl})} \geq \gamma_c, \quad i = 1, \dots, N_{\text{ue}} \quad (42c)$$

$$P_k \leq P_{\text{tx}}, \quad k = 1, \dots, N_{\text{tx}}. \quad (42d)$$

Let us define the objective function as $f(\boldsymbol{\rho}, t) = \frac{\boldsymbol{\rho}^T \mathbf{A}_r \boldsymbol{\rho}}{t}$ in terms of the optimization variable $\left[\boldsymbol{\rho}^T \quad t \right]^T$. The function $f(\boldsymbol{\rho}, t)$ is a convex function (the proof is given in Appendix D).

Utilizing the convexity of the objective function and utilizing the first-order Taylor approximation around the previous iterate $(\boldsymbol{\rho}^{(c-1)}, t^{(c-1)})$, where c is the iteration counter, the objective function is lower bounded as

$$f(\boldsymbol{\rho}, t) \geq f(\boldsymbol{\rho}^{(c-1)}, t^{(c-1)}) + \left(\begin{bmatrix} \boldsymbol{\rho} \\ t \end{bmatrix} - \begin{bmatrix} \boldsymbol{\rho}^{(c-1)} \\ t^{(c-1)} \end{bmatrix} \right)^T \nabla f(\boldsymbol{\rho}^{(c-1)}, t^{(c-1)}). \quad (43)$$

At iteration c , instead of the actual objective function, we maximize its lower bound according to the concave-convex procedure. After removing the constant terms that are independent of the optimization variables in use, we obtain the linearized objective function to be maximized as

$$\begin{aligned} \begin{bmatrix} \boldsymbol{\rho} \\ t \end{bmatrix}^T \nabla f(\boldsymbol{\rho}^{(c-1)}, t^{(c-1)}) &= \begin{bmatrix} \boldsymbol{\rho} \\ t \end{bmatrix}^T \begin{bmatrix} \frac{2\mathbf{A}_r \boldsymbol{\rho}^{(c-1)}}{t^{(c-1)}} \\ -\frac{(\boldsymbol{\rho}^{(c-1)})^T \mathbf{A}_r \boldsymbol{\rho}^{(c-1)}}{(t^{(c-1)})^2} \end{bmatrix} \\ &= \frac{2\boldsymbol{\rho}^T \mathbf{A}_r \boldsymbol{\rho}^{(c-1)}}{t^{(c-1)}} - \frac{(\boldsymbol{\rho}^{(c-1)})^T \mathbf{A}_r \boldsymbol{\rho}^{(c-1)}}{(t^{(c-1)})^2} t \\ &= \left(2\boldsymbol{\rho} - \frac{t}{t^{(c-1)}} \boldsymbol{\rho}^{(c-1)}\right)^T \left(\frac{\mathbf{A}_r \boldsymbol{\rho}^{(c-1)}}{t^{(c-1)}}\right). \end{aligned} \quad (44)$$

Now, the optimization problem can be rewritten as

$$\underset{\boldsymbol{\rho} \geq \mathbf{0}, t}{\text{minimize}} \quad - \left(2\boldsymbol{\rho} - \frac{t}{t^{(c-1)}} \boldsymbol{\rho}^{(c-1)}\right)^T \left(\frac{\mathbf{A}_r \boldsymbol{\rho}^{(c-1)}}{t^{(c-1)}}\right) \quad (45a)$$

$$\text{subject to} \quad (42b), (42c), (42d). \quad (45b)$$

The quadratic constraints in (42b) are convex and the communication SINR constraints in (42c) can be rewritten as second-order cone (SOC) constraints in terms of $\boldsymbol{\rho} = [\sqrt{\rho_0} \ \dots \ \sqrt{\rho_{N_{\text{ue}}}}]^T$ as

$$\left\| \begin{bmatrix} a_{i,0} \sqrt{\rho_0} & a_{i,1} \sqrt{\rho_1} & \dots & a_{i,i} \sqrt{\rho_i} & \dots & \dots & a_{i,N_{\text{ue}}} \sqrt{\rho_{N_{\text{ue}}}} & \sigma_n \end{bmatrix} \right\| \leq \frac{\sqrt{\rho_i} b_i}{\sqrt{\gamma_c}}, \quad i = 1, \dots, N_{\text{ue}}, \quad (46)$$

where

$$b_i = |\mathbb{E} \{ \mathbf{h}_i^H \mathbf{w}_i \} |, \quad i = 1, \dots, N_{\text{ue}} \quad (47)$$

$$a_{i,0} = \sqrt{\mathbb{E} \left\{ \left| \tilde{\mathbf{h}}_i^H \mathbf{w}_0 \right|^2 \right\}}, \quad i = 1, \dots, N_{\text{ue}} \quad (48)$$

$$a_{i,j} = \sqrt{\mathbb{E} \left\{ \left| \mathbf{h}_i^H \mathbf{w}_j \right|^2 \right\}}, \quad i = 1, \dots, N_{\text{ue}}, \quad j = 1, \dots, N_{\text{ue}}, \quad j \neq i \quad (49)$$

$$a_{i,i} = \sqrt{\mathbb{E} \left\{ \left| \mathbf{h}_i^H \mathbf{w}_i \right|^2 \right\} - b_i^2}, \quad i = 1, \dots, N_{\text{ue}} \quad (50)$$

from (14). The third set of constraints in (42d) can also be rewritten in SOC form as

$$\|\mathbf{F}_k \boldsymbol{\rho}\| \leq \sqrt{P_{\text{tx}}}, \quad k = 1, \dots, N_{\text{tx}} \quad (51)$$

where $\mathbf{F}_k = \text{diag} \left(\sqrt{\mathbb{E} \{ \|\mathbf{w}_{0,k}\|^2 \}}, \dots, \sqrt{\mathbb{E} \{ \|\mathbf{w}_{N_{\text{ue}},k}\|^2 \}} \right)$ from (4). Now, the optimization problem in (45) can be expressed as a concave-convex programming problem as

$$\underset{\boldsymbol{\rho} \geq \mathbf{0}, t}{\text{minimize}} \quad - \left(2\boldsymbol{\rho} - \frac{t}{t^{(c-1)}} \boldsymbol{\rho}^{(c-1)}\right)^T \left(\frac{\mathbf{A}_r \boldsymbol{\rho}^{(c-1)}}{t^{(c-1)}}\right) \quad (52a)$$

$$\text{subject to} \quad (42b), (46), (51). \quad (52b)$$

Algorithm 1 Concave-Convex Procedure for Power Allocation

- 1: **Initialization:** Set an arbitrary initial positive $\boldsymbol{\rho}^{(0)}$ and the solution accuracy $\epsilon > 0$. Set the iteration counter to $c = 0$ and $t^{(0)} = \tau M N_{\text{rx}} \sigma_n^2 + (\boldsymbol{\rho}^{(0)})^T \mathbf{B}_r \boldsymbol{\rho}^{(0)}$.
 - 2: $c \leftarrow c + 1$.
 - 3: Set $\boldsymbol{\rho}^{(c)}$ and $t^{(c)}$ to the solution of the convex problem in (52), where the previous iterate $\boldsymbol{\rho}^{(c-1)}$ and $t^{(c-1)}$ are taken as constant.
 - 4: If $\left(2(\boldsymbol{\rho}^{(c)} - \boldsymbol{\rho}^{(c-1)}) - \frac{t^{(c)} - t^{(c-1)}}{t^{(c-1)}} \boldsymbol{\rho}^{(c-1)} \right)^T \mathbf{A}_r \frac{\boldsymbol{\rho}^{(c-1)}}{t^{(c-1)}} \leq \epsilon$, terminate the iterations. Otherwise return to Step 2.
 - 5: **Output:** The transmit power coefficients $\boldsymbol{\rho}^{(c)}$.
-

This problem can be solved using the concave-convex procedure, whose steps are outlined in Algorithm 1. Under some mild conditions, this algorithm is guaranteed to converge to a stationary point of the problem [37].

VIII. NUMERICAL RESULTS

In this section, we provide numerical results to quantify the tradeoff between communications and sensing using the proposed MAPRT detector and power allocation algorithm. A total area of $500 \text{ m} \times 500 \text{ m}$ is considered within which UEs are randomly generated. During each sensing period, the target's location is fixed and known, but it can be anywhere within a $15 \text{ m} \times 15 \text{ m}$ sensing hotspot region located in the center of the area. The interference $\rho_0 \mathbb{E}\{|\tilde{\mathbf{h}}_i^H \mathbf{w}_0|^2\}$ created by the sensing beams to the UEs in (14) is computed by averaging over 1000 target locations in this region. We assume that the $N_{\text{tx}} + N_{\text{rx}}$ APs are also uniformly generated in the network area; however, they are fixed during the simulation. The number of transmitter APs is $N_{\text{tx}} = 16$. The $N_{\text{rx}} = 2$ closest APs to the sensing hotspot area are selected as the sensing receivers. The 2D locations of all the APs and the target are illustrated in Fig 2. In our simulation, we consider a total of $N_{\text{ue}} = 8$ UEs.

The maximum transmit power per AP is 1 W and the uplink pilot transmission power is 0.2 W. The path loss for the communication channels and the target-free channels are modeled by the 3GPP Urban Microcell model, defined in [38, Table B.1.2.1-1], with the difference that for the latter the channel gains are multiplied by an additional scaling parameter, $\varsigma \in (0, 1)$ to suppress the known parts of the target-free channels due to LOS and permanent obstacles. Hence, the higher the value of ς is, the stronger the clutter power is. On the other hand, the sensing channel

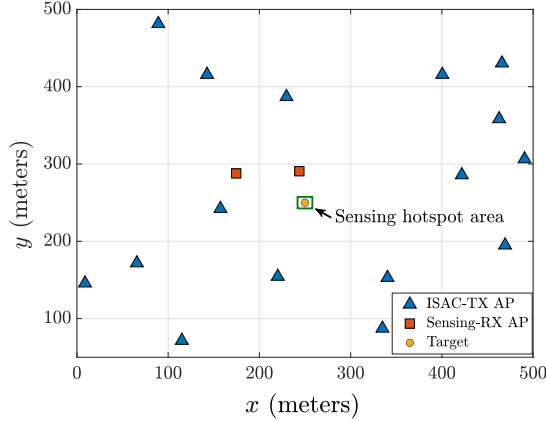


Fig. 2. The 2D locations of the APs and the target.

gains are computed by (16). The carrier frequency, the bandwidth, and the noise variance are set to 1.9 GHz, 20 MHz, and -94 dBm, respectively.

The spatial correlation matrices for the communication channels are generated by using the local scattering model in [23, Sec. 2.5.3], while the RCS of the target is modeled by the Swerling-I model where $\alpha_{r,k} \sim \mathcal{CN}(0, \sigma_{r,k}^2)$. For simplicity, we assume that the RCS values are independent and have the same variance $\sigma_{r,k}^2 = \sigma_{rcs}^2$ for each pair of transmitter AP k and receiver AP r .

The communication SINR threshold is set to 3 dB for each UE. The detection threshold, λ_d in (36), is determined based on the false alarm probability P_{fa} of either 0.1 or 0.01, which are relevant for radar applications [35] and can be improved more by using specific techniques [32]. We use the MAPRT detector with a sensing period equal to the transmission time of τ symbols out of a total of $\tau_c = 200$ symbols per coherence interval with $\tau_p = 10$. The sensing period, τ , is set to 10 and the scaling parameter ε is set to 0.3 unless otherwise stated. Note that the number of samples used for sensing depends on several factors, such as the angular range and time interval for beam scanning in the sensing hotspot region [32]. When the sensing channel gain is lower due to the undesired atmospheric conditions or a smaller false alarm probability is required, then more symbols would be needed to achieve the same detection probability. In this paper, the parameters are selected to cover a large range of RCS and detection probability values for a comprehensive comparison between several methods. Ultimately, it is possible to enhance a given detection probability to elevated levels through the application of certain methods [32].

The detection probability, P_d , is computed by averaging over 100 random UE locations and channel realizations. For each set of UE locations, the expectations in (14) are obtained by taking average over 1000 random channel realizations. In each setup, $\frac{10^2}{P_{fa}}$ random RCS and

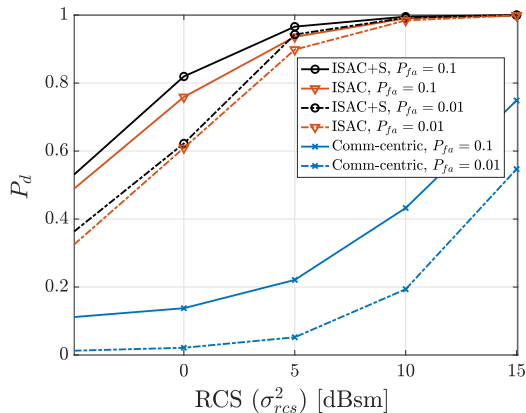


Fig. 3. P_d vs. RCS variance for $\varsigma = 0.3$, $P_{fa} = 0.1, 0.01$.

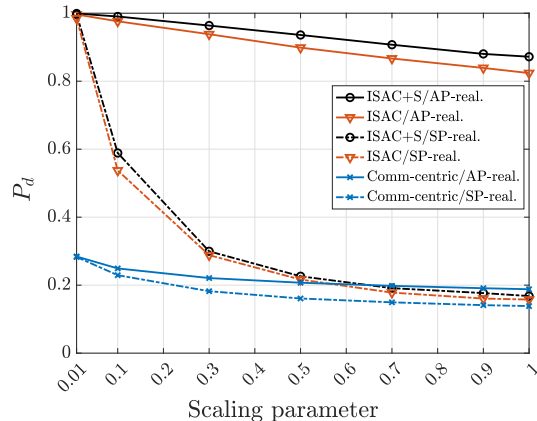


Fig. 4. P_d vs. scaling parameter ς for $\sigma_{rcs}^2 = 5$ dBsm and $P_{fa} = 0.1$.

$\frac{10^2}{P_{fa}} \cdot \tau$ random noise realizations are taken into consideration for accurate estimation of P_d .

To evaluate the efficiency of the proposed power allocation algorithm, a communication-centric approach is utilized as the baseline algorithm. The objective of the baseline algorithm is to minimize the total power consumption subject to the same constraints as the proposed algorithm. Conversely, the proposed algorithm aims to maximize the sensing SINR. Therefore, three algorithms are compared in this section: i) the communication-centric (*comm.-centric*); ii) the proposed ISAC power allocation algorithm ii.a) without additional sensing symbols (*ISAC*) and ii.b) with dedicated additional sensing symbols (*ISAC+S*). We also compare the performance of the proposed power allocation and sensing algorithms in both *realistic* and *idealistic* scenarios. The former corresponds to the described system model with target-free channels that cannot be canceled at the receiver APs, while the latter is for the case that target-free channels can be completely suppressed.

Moreover, we investigate the performance of the algorithms in relation to the consideration of target-free channels during processing. The *simple processing (SP)* approach, as described in our previous work [25], represents the scenario when the target-free channels are disregarded. In contrast, the *advanced processing (AP)* approach considers the target-free channels in deriving the test statistics and optimizing power allocation as done in this paper. In both cases, the communication channels are estimated using the uplink pilots.

Fig. 3 shows the detection probability versus the variance of the RCS for false alarm probabilities of 0.1 and 0.01. The results demonstrate that increasing the false alarm probability leads to increased detection probability. This is because a higher false alarm probability implies a lower threshold, resulting in a higher detection probability. However, for both false alarm probabilities

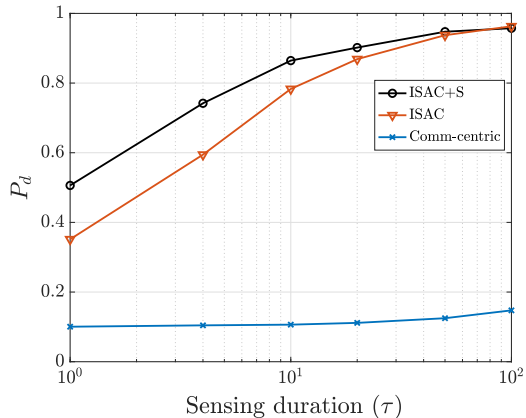


Fig. 5. P_d vs. sensing duration τ for $\varepsilon = 0.01$, $P_{fa} = 0.1$, and $\sigma_{r_{cs}}^2 = -10$ dBsm.

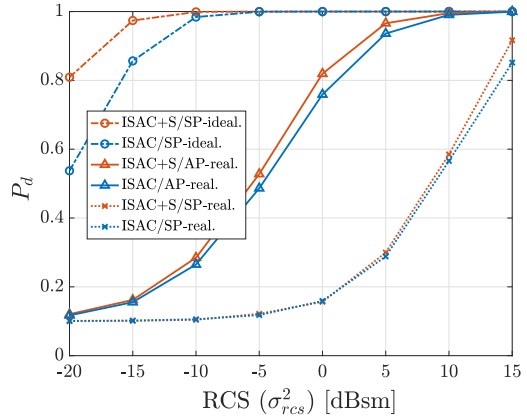


Fig. 6. P_d vs. RCS variance for $P_{fa} = 0.1$ and $\varepsilon = 0.3$.

0.1 and 0.01, the proposed *ISAC* and *ISAC+S* algorithms can achieve a detection probability close to 1 when the RCS variance is ≥ 10 dBsm (“dBsm” is the unit of RCS variance expressed in decibels relative to a square meter). In contrast, the *comm-centric* algorithm fails to attain a P_d above 0.8 due to not considering the sensing requirements. The detection probability also tends to increase as the RCS variance increases. In addition, the *ISAC+S* algorithm supports lower RCS variances, about 1 dB lower than that of *ISAC*, for a specific P_d .

The effect of the unknown target-free channels on the detection probability is investigated in Fig. 4, which illustrates the detection probability versus scaling parameter, ε , for simple and advanced processing. The scaling parameter ε affects the interference from the unknown part of the target-free channels. When $\varepsilon = 1$, no information about the target-free channels is available, which makes them impossible to be suppressed. As expected, reducing ε leads to an improved detection probability, as the interference power for sensing signals decreases with a lower value of ε . More importantly, the efficiency of advanced processing that exploits the statistics of the target-free channels in *realistic* scenarios has been shown since there is a significant gap between the performance of both proposed algorithms, *ISAC* and *ISAC+S*, with *AP* and *SP*. The results also show that the proposed scheme is quite robust to the power increase in the unknown part of the target-free channel.

The detection probability versus the sensing duration τ is depicted in Fig. 5. In general, increasing τ improves the sensing performance of all algorithms, although the proposed algorithm with additional sensing beams, *ISAC+S*, outperforms the two other algorithms. However, it is worth noting that the proposed algorithm without additional sensing beams (i.e., *ISAC*) converges to the performance of *ISAC+S* algorithm when τ is greater than 50.

Finally, the efficiency of the proposed algorithms in both *realistic* and *idealistic* scenarios, with simple and advanced processing, is investigated in terms of RCS variance in Fig. 6. The results demonstrate that *SP-real*. provides a lower bound, while the performance of *SP-ideal*. serves as an upper bound. In the realistic scenario, there is a substantial gap between the use of simple processing and advanced processing. However, for high RCS variances, simple processing can reach high performance. Moreover, the performance of simple processing would be better for lower scaling parameters (see Fig. 4). This implies that when the target has good reflectivity and the interference coming from unknown target-free channels is low, we can ignore the target-free channels and use simple processing, which is more computationally friendly than advanced processing.

IX. CONCLUSION

An ISAC framework in a cell-free massive MIMO is proposed for downlink communication with imperfect CSI, as well as, multi-static target detection in the presence of clutter. A MAPRT detector is developed to detect the target with a known location but unknown RCS using centralized processing. A power allocation algorithm is proposed to maximize the sensing SINR while satisfying both communication and per-AP power constraints to improve the ISAC performance. Numerical results show that, compared to a fully communication-centric algorithm, and in the presence of clutter, a significant improvement in detection probability can be achieved by the proposed algorithm with and without additional sensing beams. However, the use of additional sensing beams further supports lower RCS variances. Moreover, a significant gap has been observed between the performance of the proposed algorithms, which exploit the statistics of the target-free channels, and the one in which these channels are ignored in the processing. However, this gap becomes smaller when the clutter power reduces, and the RCS variance is relatively high facilitating computationally simpler target detection.

APPENDIX A

PROOF OF LEMMA 1

By noting that only the effective channel $\mathbb{E}\{\mathbf{h}_i^H \mathbf{w}_i\}$ is known at UE i , Equation (12) can be rewritten as

$$y_i[m] = \underbrace{\sqrt{\rho_i} \mathbb{E}\{\mathbf{h}_i^H \mathbf{w}_i\}}_{\text{Desired signal}} s_i[m] + \underbrace{\nu_i[m]}_{\text{Interference}} + \underbrace{n_i[m]}_{\text{Noise}}, \quad (53)$$

where

$$\begin{aligned}
\nu_i[m] = & \underbrace{\sqrt{\rho_i} (\mathbf{h}_i^H \mathbf{w}_i - \mathbb{E} \{ \mathbf{h}_i^H \mathbf{w}_i \}) s_i[m]}_{\text{Self-interference signal due to the unknown part of the channel}} + \underbrace{\sum_{j=1, j \neq i}^{N_{\text{ue}}} \sqrt{\rho_j} \mathbf{h}_i^H \mathbf{w}_j s_j[m]}_{\text{Interference signal due to the other UEs}} \\
& + \underbrace{\sqrt{\rho_0} \mathbf{h}_i^H \mathbf{w}_0 s_0[m]}_{\text{Interference signal due to the sensing}}. \tag{54}
\end{aligned}$$

The interference signal $\nu_i[m]$ has zero mean since s_i and s_0 have zero means. Moreover, it is uncorrelated with the desired symbol $s_i[m]$ since

$$\mathbb{E} \{ \nu_i[m] s_i^*[m] \} = \sqrt{\rho_i} \underbrace{\mathbb{E} \{ \mathbf{h}_i^H \mathbf{w}_i - \mathbb{E} \{ \mathbf{h}_i^H \mathbf{w}_i \} \}}_{=0} \mathbb{E} \{ |s_i[m]|^2 \} = 0. \tag{55}$$

Following Lemma 3.3 and Theorem 6.1 in [23], the achievable SE of UE i can be obtained as in (13). Note that \mathbf{w}_0 is designed in the nullspace of the estimated channel vectors, and, thus, $\hat{\mathbf{h}}_i^H \mathbf{w}_0 = 0$, for $i = 1, \dots, N_{\text{ue}}$. Therefore, the interference power due to the sensing signal is only coming from the channel estimation error, $\tilde{\mathbf{h}}_i$, i.e.,

$$\mathbb{E} \{ |\mathbf{h}_i^H \mathbf{w}_0|^2 \} = \mathbb{E} \{ |\tilde{\mathbf{h}}_i^H \mathbf{w}_0|^2 \}. \tag{56}$$

APPENDIX B

PROOF OF LEMMA 2

A. Optimization under \mathcal{H}_0

Given that the hypothesis \mathcal{H}_0 is true, we have $\mathbf{y}_\tau = \mathbf{h}_\tau + \mathbf{n}_\tau$. In order to solve the optimization problem under \mathcal{H}_0 , we first derive the conditional PDF of \mathbf{y}_τ given the target-free channel vector \mathbf{h} and the hypothesis \mathcal{H}_0 and PDF of \mathbf{h} in (28) as

$$p(\mathbf{y}_\tau | \mathbf{h}, \mathcal{H}_0) = p(\mathbf{n}_\tau = \mathbf{y}_\tau - \mathbf{h}_\tau | \mathbf{h}) = \underbrace{\frac{1}{(\pi \sigma_n^2)^{MN_{\text{rx}}\tau}}}_{\triangleq C_1} \exp \left(- \sum_{m=1}^{\tau} \frac{\|\mathbf{y}[m] - \mathbf{X}[m]\mathbf{h}\|^2}{\sigma_n^2} \right), \tag{57}$$

$$p(\mathbf{h} | \mathcal{H}_0) = p(\mathbf{h}) = \underbrace{\frac{1}{\pi^{M^2 N_{\text{tx}} N_{\text{rx}}} \det(\mathbf{R})}}_{\triangleq C_2} \exp(-\mathbf{h}^H \mathbf{R}^{-1} \mathbf{h}), \tag{58}$$

respectively, where we have defined $C_1 = \frac{1}{(\pi \sigma_n^2)^{MN_{\text{rx}}\tau}}$ and $C_2 = \frac{1}{\pi^{M^2 N_{\text{tx}} N_{\text{rx}}} \det(\mathbf{R})}$. Note that \mathbf{h} is independent of the hypothesis \mathcal{H}_0 . Now, the optimization under \mathcal{H}_0 can be rewritten as

$$\Lambda_{\text{den}} = \max_{\mathbf{h}} C_1 C_2 \exp \left(- \sum_{m=1}^{\tau} \frac{\|\mathbf{y}[m] - \mathbf{X}[m]\mathbf{h}\|^2}{\sigma_n^2} - \mathbf{h}^H \mathbf{R}^{-1} \mathbf{h} \right), \tag{59}$$

which is equivalent to

$$\Lambda_{\text{den}} = C_1 C_2 \exp \left(-\frac{1}{\sigma_n^2} \min_{\mathbf{h}} f_{\mathcal{H}_0}(\mathbf{h}) \right), \quad (60)$$

where

$$\begin{aligned} f_{\mathcal{H}_0}(\mathbf{h}) &= \mathbf{h}^H \left(\underbrace{\sum_{m=1}^{\tau} \mathbf{X}^H[m] \mathbf{X}[m] + \sigma_n^2 \mathbf{R}^{-1}}_{=\mathbf{D}} \right) \mathbf{h} - 2\Re \left(\mathbf{h}^H \underbrace{\sum_{m=1}^{\tau} \mathbf{X}^H[m] \mathbf{y}[m]}_{=\mathbf{b}} \right) + \underbrace{\sum_{m=1}^{\tau} \|\mathbf{y}[m]\|^2}_{=F} \\ &= \mathbf{h}^H \mathbf{D} \mathbf{h} - \mathbf{h}^H \mathbf{b} - \mathbf{b}^H \mathbf{h} + F, \end{aligned} \quad (61)$$

where \mathbf{D} , \mathbf{b} , and F are given in (32), (31), and (33), respectively. Then, the estimate of the vectorized target-free channel \mathbf{h} that minimizes the quadratic convex objective function $f_{\mathcal{H}_0}(\mathbf{h})$ in (60) is obtained as $\hat{\mathbf{h}} = \mathbf{D}^{-1} \mathbf{b}$. Finally, substituting the optimally estimated $\hat{\mathbf{h}}$ into $f_{\mathcal{H}_0}(\mathbf{h})$ in (60), we obtain the denominator of the likelihood ratio in (26) as in (29).

B. Optimization under \mathcal{H}_1

Given that the hypothesis \mathcal{H}_1 is true, we have $\mathbf{y}_\tau = \mathbf{g}_\tau + \mathbf{h}_\tau + \mathbf{n}_\tau$. Then, the conditional PDF of \mathbf{y}_τ given α , \mathbf{h} and the hypothesis \mathcal{H}_1 is obtained as

$$p(\mathbf{y}_\tau | \alpha, \mathbf{h}, \mathcal{H}_1) = p(\mathbf{n}_\tau = \mathbf{y}_\tau - \mathbf{g}_\tau - \mathbf{h}_\tau | \alpha, \mathbf{h}) = C_1 \exp \left(-\sum_{m=1}^{\tau} \frac{\|\mathbf{y}[m] - \mathbf{G}[m] \alpha - \mathbf{X}[m] \mathbf{h}\|^2}{\sigma_n^2} \right). \quad (62)$$

Note that \mathbf{h} and α are independent of the hypothesis \mathcal{H}_1 . Therefore, $p(\mathbf{h} | \mathcal{H}_1) = p(\mathbf{h})$ which is given in (58) and the conditional PDF of α given the hypothesis \mathcal{H}_1 is equal to its PDF given as

$$p(\alpha | \mathcal{H}_1) = p(\alpha) = C_3 \exp(-\alpha^H \mathbf{R}_{\text{rcs}}^{-1} \alpha), \quad (63)$$

where $C_3 = \frac{1}{\pi^{N_{\text{tx}} N_{\text{rx}}} \det(\mathbf{R}_{\text{rcs}})}$. Now, we can rewrite (27) as

$$\Lambda_{\text{num}} = C_1 C_2 C_3 \exp \left(-\frac{1}{\sigma_n^2} \min_{\alpha, \mathbf{h}} f_{\mathcal{H}_1}(\alpha, \mathbf{h}) \right), \quad (64)$$

where

$$\begin{aligned} f_{\mathcal{H}_1}(\alpha, \mathbf{h}) &= \sum_{m=1}^{\tau} \|\mathbf{y}[m] - \mathbf{G}[m] \alpha - \mathbf{X}[m] \mathbf{h}\|^2 + \alpha^H \sigma_n^2 \mathbf{R}_{\text{rcs}}^{-1} \alpha + \mathbf{h}^H \sigma_n^2 \mathbf{R}^{-1} \mathbf{h} \\ &= \underbrace{\sum_{m=1}^{\tau} \|\mathbf{y}[m]\|^2}_F - 2\Re \left(\alpha^H \underbrace{\sum_{m=1}^{\tau} \mathbf{G}^H[m] \mathbf{y}[m]}_{\mathbf{a}} \right) - 2\Re \left(\mathbf{h}^H \underbrace{\sum_{m=1}^{\tau} \mathbf{X}^H[m] \mathbf{y}[m]}_{\mathbf{b}} \right) \end{aligned}$$

$$\begin{aligned}
& + \boldsymbol{\alpha}^H \underbrace{\left(\sum_{m=1}^{\tau} \mathbf{G}^H[m] \mathbf{G}[m] + \sigma_n^2 \mathbf{R}_{\text{rcs}}^{-1} \right)}_{\mathbf{C}} \boldsymbol{\alpha} + \mathbf{h}^H \underbrace{\left(\sum_{m=1}^{\tau} \mathbf{X}^H[m] \mathbf{X}[m] + \sigma_n^2 \mathbf{R}^{-1} \right)}_{\mathbf{D}} \mathbf{h} \\
& + 2\Re \left(\underbrace{\boldsymbol{\alpha}^H \sum_{m=1}^{\tau} \mathbf{G}^H[m] \mathbf{X}[m] \mathbf{h}}_{\mathbf{E}} \right). \tag{65}
\end{aligned}$$

In (65), the vectors \mathbf{a} and \mathbf{b} , the matrices \mathbf{C} , \mathbf{D} , and \mathbf{E} , and the scalar F are given in (31), (32), and (33), respectively. The objective function in (65) can be rewritten as

$$f_{\mathcal{H}_1}(\boldsymbol{\alpha}, \mathbf{h}) = \begin{bmatrix} \boldsymbol{\alpha}^H & \mathbf{h}^H \end{bmatrix} \begin{bmatrix} \mathbf{C} & \mathbf{E} \\ \mathbf{E}^H & \mathbf{D} \end{bmatrix} \begin{bmatrix} \boldsymbol{\alpha} \\ \mathbf{h} \end{bmatrix} - 2\Re \left(\begin{bmatrix} \boldsymbol{\alpha}^H & \mathbf{h}^H \end{bmatrix} \begin{bmatrix} \mathbf{a} \\ \mathbf{b} \end{bmatrix} \right) + F. \tag{66}$$

Equating the first derivative of $f_{\mathcal{H}_1}(\boldsymbol{\alpha}, \mathbf{h})$ with respect to $\boldsymbol{\alpha}^H$ and \mathbf{h}^H to zero, the estimated $\boldsymbol{\alpha}$ and \mathbf{h} are obtained as

$$\begin{bmatrix} \hat{\boldsymbol{\alpha}} \\ \hat{\mathbf{h}} \end{bmatrix} = \begin{bmatrix} \mathbf{C} & \mathbf{E} \\ \mathbf{E}^H & \mathbf{D} \end{bmatrix}^{-1} \begin{bmatrix} \mathbf{a} \\ \mathbf{b} \end{bmatrix}. \tag{67}$$

Substituting (67) in (66), we have

$$\min_{\boldsymbol{\alpha}, \mathbf{h}} f_{\mathcal{H}_1}(\boldsymbol{\alpha}, \mathbf{h}) = - \begin{bmatrix} \mathbf{a}^H & \mathbf{b}^H \end{bmatrix} \begin{bmatrix} \mathbf{C} & \mathbf{E} \\ \mathbf{E}^H & \mathbf{D} \end{bmatrix}^{-1} \begin{bmatrix} \mathbf{a} \\ \mathbf{b} \end{bmatrix} + F. \tag{68}$$

Then, the numerator of the likelihood ratio in (26) is derived by inserting (68) into (64) and given in (30).

APPENDIX C

PROOF OF SENSING SINR

The sensing SINR for the received vector signal in (24) is given as

$$\text{SINR}_s = \frac{\mathbb{E} \{ \|\mathbf{g}_\tau\|^2 \}}{\mathbb{E} \{ \|\mathbf{n}_\tau\|^2 \} + \mathbb{E} \{ \|\mathbf{h}_\tau\|^2 \}} = \frac{\sum_{m=1}^{\tau} \mathbb{E} \{ \|\mathbf{G}[m] \boldsymbol{\alpha}\|^2 \}}{\tau M N_{\text{rx}} \sigma_n^2 + \sum_{m=1}^{\tau} \mathbb{E} \{ \|\mathbf{X}[m] \mathbf{h}\|^2 \}}. \tag{69}$$

Using (15), the expectation $\mathbb{E} \{ \|\mathbf{G}[m] \boldsymbol{\alpha}\|^2 \}$ in the numerator can be computed as

$$\begin{aligned}
\mathbb{E} \{ \|\mathbf{G}[m] \boldsymbol{\alpha}\|^2 \} &= \sum_{r=1}^{N_{\text{rx}}} \mathbb{E} \left\{ \left\| \sum_{k=1}^{N_{\text{tx}}} \alpha_{r,k} \mathbf{g}_{r,k}[m] \right\|^2 \right\} = \sum_{r=1}^{N_{\text{rx}}} \sum_{k=1}^{N_{\text{tx}}} \sum_{j=1}^{N_{\text{tx}}} \mathbb{E} \{ \mathbf{g}_{r,k}^H[m] \alpha_{r,k}^* \alpha_{r,j} \mathbf{g}_{r,j}[m] \} \\
&\stackrel{(a)}{=} \sum_{r=1}^{N_{\text{rx}}} \sum_{k=1}^{N_{\text{tx}}} \sum_{j=1}^{N_{\text{tx}}} \mathbf{g}_{r,k}^H[m] \text{cov}(\alpha_{r,j}, \alpha_{r,k}) \mathbf{g}_{r,j}[m] \stackrel{(b)}{=} \boldsymbol{\rho}^T \mathbf{D}_s^H[m] \left(\sum_{r=1}^{N_{\text{rx}}} \sum_{k=1}^{N_{\text{tx}}} \sum_{j=1}^{N_{\text{tx}}} \sqrt{\beta_{r,k} \beta_{r,j}} \mathbf{W}_k^H \mathbf{a}^*(\varphi_k, \vartheta_k) \right. \\
&\quad \left. \times \mathbf{a}^H(\phi_r, \theta_r) \text{cov}(\alpha_{r,j}, \alpha_{r,k}) \mathbf{a}(\phi_r, \theta_r) \mathbf{a}^T(\varphi_j, \vartheta_j) \mathbf{W}_j \right) \mathbf{D}_s[m] \boldsymbol{\rho}, \tag{70}
\end{aligned}$$

where in (a), we treat $\mathbf{g}_{r,k}[m]$ as deterministic since the edge cloud knows $\mathbf{x}_k[m]$. In (b), we recalled the definition of $\mathbf{g}_{r,k}[m]$ from (15) and $\mathbf{x}_k[m]$ from (2). Defining

$$\mathbf{A} = \sum_{m=1}^{\tau} \mathbf{D}_s^H[m] \left(\sum_{r=1}^{N_{\text{rx}}} \sum_{k=1}^{N_{\text{tx}}} \sum_{j=1}^{N_{\text{tx}}} \sqrt{\beta_{r,k}\beta_{r,j}} \mathbf{W}_k^H \mathbf{a}^*(\varphi_k, \vartheta_k) \mathbf{a}^H(\phi_r, \theta_r) \right. \\ \left. \times \text{cov}(\alpha_{r,j}, \alpha_{r,k}) \mathbf{a}(\phi_r, \theta_r) \mathbf{a}^T(\varphi_j, \vartheta_j) \mathbf{W}_j \right) \mathbf{D}_s[m], \quad (71)$$

the term $\sum_{m=1}^{\tau} \mathbb{E} \{ \|\mathbf{G}[m]\boldsymbol{\alpha}\|^2 \}$ in the numerator of the sensing SINR in (69) can be written as $\sum_{m=1}^{\tau} \mathbb{E} \{ \|\mathbf{G}[m]\boldsymbol{\alpha}\|^2 \} = \boldsymbol{\rho}^T \mathbf{A} \boldsymbol{\rho}$.

Using (15), the expectation $\mathbb{E} \{ \|\mathbf{X}[m]\mathbf{h}\|^2 \}$ in the denominator of the sensing SINR in (69) can be expressed as

$$\mathbb{E} \{ \|\mathbf{X}[m]\mathbf{h}\|^2 \} = \sum_{r=1}^{N_{\text{rx}}} \mathbb{E} \left\{ \left\| \sum_{k=1}^{N_{\text{tx}}} \mathbf{H}_{r,k} \mathbf{x}_k[m] \right\|^2 \right\} \stackrel{(a)}{=} \sum_{r=1}^{N_{\text{rx}}} \sum_{k=1}^{N_{\text{tx}}} \sum_{j=1}^{N_{\text{tx}}} \mathbf{x}_k^H[m] \mathbb{E} \{ \mathbf{H}_{r,k}^H \mathbf{H}_{r,j} \} \mathbf{x}_j[m] \\ \stackrel{(b)}{=} \sum_{r=1}^{N_{\text{rx}}} \sum_{k=1}^{N_{\text{tx}}} \mathbf{x}_k^H[m] \mathbb{E} \{ \mathbf{H}_{r,k}^H \mathbf{H}_{r,k} \} \mathbf{x}_k[m] \stackrel{(c)}{=} \boldsymbol{\rho}^T \mathbf{D}_s^H[m] \left(\sum_{r=1}^{N_{\text{rx}}} \sum_{k=1}^{N_{\text{tx}}} \mathbf{W}_k^H \underbrace{\mathbb{E} \{ \mathbf{H}_{r,k}^H \mathbf{H}_{r,k} \}}_{\triangleq \mathfrak{R}_{r,k}} \mathbf{W}_k \right) \mathbf{D}_s[m] \boldsymbol{\rho}, \quad (72)$$

where we treat $\mathbf{x}_k[m]$ as deterministic in (a) since it is known in the edge cloud. In (b), we have used that zero-mean channels $\mathbf{H}_{r,k}$ are independent for different k and in (c) we recalled the definition of $\mathbf{x}_k[m]$ from (2). Using the correlated Rayleigh modeling of the channel $\mathbf{H}_{r,k}$ from (18), the defined expectation term $\mathfrak{R}_{r,k} = \mathbb{E} \{ \mathbf{H}_{r,k}^H \mathbf{H}_{r,k} \}$ can be written as

$$\mathfrak{R}_{r,k} = \mathbb{E} \left\{ \left(\mathbf{R}_{\text{tx},(r,k)}^{\frac{1}{2}} \right)^* \mathbf{W}_{\text{ch},(r,k)}^H \left(\mathbf{R}_{\text{rx},(r,k)}^{\frac{1}{2}} \right)^H \mathbf{R}_{\text{rx},(r,k)}^{\frac{1}{2}} \mathbf{W}_{\text{ch},(r,k)} \left(\mathbf{R}_{\text{tx},(r,k)}^{\frac{1}{2}} \right)^T \right\} \\ = \left(\mathbf{R}_{\text{tx},(r,k)}^{\frac{1}{2}} \right)^* \mathbb{E} \left\{ \mathbf{W}_{\text{ch},(r,k)}^H \mathbf{R}_{\text{rx},(r,k)} \mathbf{W}_{\text{ch},(r,k)} \right\} \left(\mathbf{R}_{\text{tx},(r,k)}^{\frac{1}{2}} \right)^T, \quad (73)$$

where we used that the square root of the positive semi-definite matrix $\mathbf{R}_{\text{rx},(r,k)}$ is Hermitian symmetric. The (m, n) th entry of the matrix $\mathbb{E} \left\{ \mathbf{W}_{\text{ch},(r,k)}^H \mathbf{R}_{\text{rx},(r,k)} \mathbf{W}_{\text{ch},(r,k)} \right\}$ is

$$\mathbb{E} \left\{ \left[\mathbf{W}_{\text{ch},(r,k)} \right]_{:m}^H \mathbf{R}_{\text{rx},(r,k)} \left[\mathbf{W}_{\text{ch},(r,k)} \right]_{:n} \right\} = \text{tr} \left(\mathbb{E} \left\{ \left[\mathbf{W}_{\text{ch},(r,k)} \right]_{:m}^H \mathbf{R}_{\text{rx},(r,k)} \left[\mathbf{W}_{\text{ch},(r,k)} \right]_{:n} \right\} \right) \\ = \mathbb{E} \left\{ \text{tr} \left(\mathbf{R}_{\text{rx},(r,k)} \left[\mathbf{W}_{\text{ch},(r,k)} \right]_{:n} \left[\mathbf{W}_{\text{ch},(r,k)} \right]_{:m}^H \right) \right\} = \text{tr} \left(\mathbf{R}_{\text{rx},(r,k)} \mathbb{E} \left\{ \left[\mathbf{W}_{\text{ch},(r,k)} \right]_{:n} \left[\mathbf{W}_{\text{ch},(r,k)} \right]_{:m}^H \right\} \right) \quad (74)$$

where we have used the trace operation and its cyclic shift property. In the above expression, the expectation $\mathbb{E} \left\{ \left[\mathbf{W}_{\text{ch},(r,k)} \right]_{:n} \left[\mathbf{W}_{\text{ch},(r,k)} \right]_{:m}^H \right\}$ is zero if $m \neq n$. Otherwise, if $m = n$, it is equal to the identity matrix. So, the matrix $\mathbb{E} \left\{ \mathbf{W}_{\text{ch},(r,k)}^H \mathbf{R}_{\text{rx},(r,k)} \mathbf{W}_{\text{ch},(r,k)} \right\}$ in (73) is $\text{tr}(\mathbf{R}_{\text{rx},(r,k)}) \mathbf{I}_M$.

Inserting this into (73), we obtain

$$\mathfrak{R}_{r,k} = \text{tr}(\mathbf{R}_{\text{rx},(r,k)}) \left(\mathbf{R}_{\text{tx},(r,k)}^{\frac{1}{2}} \right)^* \left(\mathbf{R}_{\text{tx},(r,k)}^{\frac{1}{2}} \right)^T = \text{tr}(\mathbf{R}_{\text{rx},(r,k)}) \mathbf{R}_{\text{tx},(r,k)}^T. \quad (75)$$

Then, the expression in (72) becomes

$$\mathbb{E} \{ \|\mathbf{X}[m]\mathbf{h}\|^2 \} = \boldsymbol{\rho}^T \mathbf{D}_s^H [m] \left(\sum_{r=1}^{N_{\text{rx}}} \sum_{k=1}^{N_{\text{tx}}} \text{tr} (\mathbf{R}_{\text{rx},(r,k)}) \mathbf{W}_k^H \mathbf{R}_{\text{tx},(r,k)}^T \mathbf{W}_k \right) \mathbf{D}_s [m] \boldsymbol{\rho}. \quad (76)$$

Now, defining

$$\mathbf{B} = \sum_{m=1}^{\tau} \mathbf{D}_s^H [m] \left(\sum_{r=1}^{N_{\text{rx}}} \sum_{k=1}^{N_{\text{tx}}} \text{tr} (\mathbf{R}_{\text{rx},(r,k)}) \mathbf{W}_k^H \mathbf{R}_{\text{tx},(r,k)}^T \mathbf{W}_k \right) \mathbf{D}_s [m], \quad (77)$$

the second term in the denominator in (69) can be expressed as $\boldsymbol{\rho}^T \mathbf{B} \boldsymbol{\rho}$. Then, we obtain the sensing SINR as

$$\text{SINR}_s = \gamma_s = \frac{\boldsymbol{\rho}^T \mathbf{A} \boldsymbol{\rho}}{\tau M N_{\text{rx}} \sigma_n^2 + \boldsymbol{\rho}^T \mathbf{B} \boldsymbol{\rho}}. \quad (78)$$

APPENDIX D

PROOF OF CONVEXITY OF $f(\boldsymbol{\rho}, t)$.

We want to show that $f(\boldsymbol{\rho}, t)$ is a convex function. First, we derive the gradient vector of function $f(\boldsymbol{\rho}, t)$ as follows

$$\nabla f(\boldsymbol{\rho}, t) = \begin{bmatrix} \frac{2\mathbf{A}_r \boldsymbol{\rho}}{t} \\ -\frac{\boldsymbol{\rho}^T \mathbf{A}_r \boldsymbol{\rho}}{t^2} \end{bmatrix}. \quad (79)$$

The Hessian matrix would be

$$\mathbf{H}(\boldsymbol{\rho}, t) = \begin{bmatrix} \frac{2\mathbf{A}_r}{t} & -\frac{2\mathbf{A}_r \boldsymbol{\rho}}{t^2} \\ -\frac{2\boldsymbol{\rho}^T \mathbf{A}_r}{t^2} & \frac{2\boldsymbol{\rho}^T \mathbf{A}_r \boldsymbol{\rho}}{t^3} \end{bmatrix}. \quad (80)$$

By showing that the Hessian matrix is positive semi-definite, we prove that the objective function $f(\boldsymbol{\rho}, t)$ is convex. The former is equivalent to showing the non-negativity of $\begin{bmatrix} \bar{\boldsymbol{\rho}}^T & \bar{t} \end{bmatrix} \mathbf{H}(\boldsymbol{\rho}, t) \begin{bmatrix} \bar{\boldsymbol{\rho}} \\ \bar{t} \end{bmatrix}$ for any selection of $\bar{\boldsymbol{\rho}}$ and \bar{t} . This product can be computed as

$$\begin{aligned} \begin{bmatrix} \bar{\boldsymbol{\rho}}^T & \bar{t} \end{bmatrix} \begin{bmatrix} \frac{2\mathbf{A}_r}{t} & -\frac{2\mathbf{A}_r \boldsymbol{\rho}}{t^2} \\ -\frac{2\boldsymbol{\rho}^T \mathbf{A}_r}{t^2} & \frac{2\boldsymbol{\rho}^T \mathbf{A}_r \boldsymbol{\rho}}{t^3} \end{bmatrix} \begin{bmatrix} \bar{\boldsymbol{\rho}} \\ \bar{t} \end{bmatrix} &= \frac{2\bar{\boldsymbol{\rho}}^T \mathbf{A}_r \bar{\boldsymbol{\rho}}}{t} - \frac{2\boldsymbol{\rho}^T \mathbf{A}_r \bar{\boldsymbol{\rho}} \bar{t}}{t^2} - \frac{2\bar{\boldsymbol{\rho}}^T \mathbf{A}_r \boldsymbol{\rho} \bar{t}}{t^2} + \frac{2\boldsymbol{\rho}^T \mathbf{A}_r \boldsymbol{\rho} \bar{t}^2}{t^3} \\ &= 2 \frac{(\bar{\boldsymbol{\rho}} - \frac{\bar{t}}{t} \boldsymbol{\rho})^T \mathbf{A}_r (\bar{\boldsymbol{\rho}} - \frac{\bar{t}}{t} \boldsymbol{\rho})}{t} \geq 0, \end{aligned} \quad (81)$$

where we have expressed the result in a quadratic form. Since \mathbf{A}_r is positive semi-definite, the above result is always non-negative. As a result, we can conclude that the Hessian matrix is positive semi-definite and the objective function is convex.

REFERENCES

- [1] F. Liu, Y. Cui, C. Masouros, J. Xu, T. X. Han, Y. C. Eldar, and S. Buzzi, “Integrated sensing and communications: Towards dual-functional wireless networks for 6G and beyond,” *IEEE J. Sel. Areas Commun.*, 2022.
- [2] A. Behravan, V. Yajnanarayana, M. F. Keskin *et al.*, “Positioning and sensing in 6G: Gaps, challenges, and opportunities,” *IEEE Veh. Technol. Mag.*, vol. 18, no. 1, pp. 40–48, 2023.
- [3] A. Liu, Z. Huang, M. Li *et al.*, “A survey on fundamental limits of integrated sensing and communication,” *IEEE Commun. Surv. Tutor.*, vol. 24, no. 2, pp. 994–1034, 2022.
- [4] J. A. Zhang, M. L. Rahman, K. Wu, X. Huang, Y. J. Guo, S. Chen, and J. Yuan, “Enabling joint communication and radar sensing in mobile networks—A survey,” *IEEE Commun. Surv. Tutor.*, vol. 24, no. 1, pp. 306–345, 2021.
- [5] T. Wild, V. Braun, and H. Viswanathan, “Joint design of communication and sensing for beyond 5G and 6G systems,” *IEEE Access*, vol. 9, pp. 30 845–30 857, 2021.
- [6] F. Liu, L. Zheng, Y. Cui, C. Masouros, A. P. Petropulu, H. Griffiths, and Y. C. Eldar, “Seventy years of radar and communications: The road from separation to integration,” *arXiv preprint arXiv:2210.00446*, 2022.
- [7] X. Liu, T. Huang, N. Shlezinger, Y. Liu, J. Zhou, and Y. C. Eldar, “Joint transmit beamforming for multiuser MIMO communications and MIMO radar,” *IEEE Trans. Signal Process.*, vol. 68, pp. 3929–3944, 2020.
- [8] J. Mu, Y. Gong, F. Zhang, Y. Cui, F. Zheng, and X. Jing, “Integrated sensing and communication-enabled predictive beamforming with deep learning in vehicular networks,” *IEEE Commun. Lett.*, vol. 25, no. 10, pp. 3301–3304, 2021.
- [9] J. Pritzker, J. Ward, and Y. C. Eldar, “Transmit precoder design approaches for dual-function radar-communication systems,” *arXiv preprint arXiv:2203.09571*, 2022.
- [10] R. Thomä, T. Dallmann, S. Jovanoska, P. Knott, and A. Schmeink, “Joint communication and radar sensing: An overview,” in *15th European Conference on Antennas and Propagation (EuCAP)*, 2021.
- [11] Y. Huang, Y. Fang, X. Li, and J. Xu, “Coordinated power control for network integrated sensing and communication,” *IEEE Trans. Veh. Technol.*, vol. 71, no. 12, pp. 13 361–13 365, 2022.
- [12] A. Zhang, M. L. Rahman, X. Huang, Y. J. Guo, S. Chen, and R. W. Heath, “Perceptive mobile networks: Cellular networks with radio vision via joint communication and radar sensing,” *IEEE Veh. Technol. Mag.*, vol. 16, no. 2, pp. 20–30, 2020.
- [13] S. Buzzi, C. D’Andrea, and M. Lops, “Using massive MIMO arrays for joint communication and sensing,” in *53rd Asilomar Conference on Signals, Systems, and Computers*, 2019, pp. 5–9.
- [14] H. Hua, J. Xu, and T. X. Han, “Transmit beamforming optimization for integrated sensing and communication,” in *IEEE Global Communications Conference (GLOBECOM)*, 2021.
- [15] M. Ye, W. Hu, Y. Zhao, L. Huang, and Z. Shi, “Beamforming design for OFDM joint sensing and communication system,” *Journal of Internet Technology*, vol. 23, no. 7, pp. 1449–1459, 2022.
- [16] Z. Liu, S. Aditya, H. Li, and B. Clerckx, “Joint transmit and receive beamforming design in full-duplex integrated sensing and communications,” *arXiv preprint arXiv:2210.10904*, 2022.
- [17] Y. He, Y. Cai, G. Yu, and K.-K. Wong, “Joint transceiver design for dual-functional full-duplex relay aided radar-communication systems,” *IEEE Trans. Commun.*, vol. 70, no. 12, pp. 8355–8369, 2022.
- [18] J. Li, G. Zhou, T. Gong, and N. Liu, “A framework for mutual information-based MIMO integrated sensing and communication beamforming design,” *arXiv preprint arXiv:2211.07887*, 2022.
- [19] J. Li and N. Liu, “Integrated sensing and communication beamforming design based on mutual information,” in *2022 IEEE/CIC International Conference on Communications in China (ICCC Workshops)*. IEEE, 2022, pp. 383–388.
- [20] S. Shi, Z. Cheng, L. Wu, Z. He, and B. Shankar, “Distributed 5G NR-based integrated sensing and communication systems: Frame structure and performance analysis,” in *EUSIPCO*, 2022, pp. 1062–1066.

- [21] F. Liu, W. Yuan, C. Masouros, and J. Yuan, "Radar-assisted predictive beamforming for vehicular links: Communication served by sensing," *IEEE Trans. Wirel. Commun.*, vol. 19, no. 11, pp. 7704–7719, 2020.
- [22] A. Bazzi and M. Chafii, "On outage-based beamforming design for dual-functional radar-communication 6G systems," *IEEE Trans. Wirel. Commun.*, 2023.
- [23] Ö. T. Demir, E. Björnson, and L. Sanguinetti, "Foundations of user-centric cell-free massive MIMO," *Foundations and Trends® in Signal Processing*, vol. 14, no. 3-4, pp. 162–472, 2021.
- [24] Ö. T. Demir, M. Masoudi, E. Björnson, and C. Cavdar, "Cell-free massive MIMO in O-RAN: Energy-aware joint orchestration of cloud, fronthaul, and radio resources," *arXiv preprint arXiv:2301.06166*, 2023.
- [25] Z. Behdad, Ö. T. Demir, K. W. Sung, E. Björnson, and C. Cavdar, "Power allocation for joint communication and sensing in cell-free massive MIMO," in *IEEE Global Communications Conference (GLOBECOM)*, 2022, pp. 4081–4086.
- [26] S. Buzzi, C. D'Andrea, and M. Lops, "Transmit power allocation for joint communication and sensing through massive MIMO arrays," in *WSA 2020; 24th International ITG Workshop on Smart Antennas*, 2020.
- [27] A. Sakhnini, M. Guenach, A. Bourdoux, H. Sahli, and S. Pollin, "A target detection analysis in cell-free massive MIMO joint communication and radar systems," in *IEEE International Conference on Communications*, 2022, pp. 2567–2572.
- [28] U. Demirhan and A. Alkhateeb, "Cell-free ISAC MIMO systems: Joint sensing and communication beamforming," *arXiv preprint arXiv:2301.11328*, 2023.
- [29] Y. Guo, C. Li, C. Zhang, Y. Yao, and B. Xia, "Performance analysis of the full-duplex communicating-radar convergence system," *arXiv preprint arXiv:2210.12358*, 2022.
- [30] Z. Zhang, Q. Chang, S. Yang, and J. Xing, "Sensing-communication bandwidth allocation in vehicular links based on reinforcement learning," *IEEE Wireless Communications Letters*, vol. 12, no. 1, pp. 11–15, 2023.
- [31] G. Cheng and J. Xu, "Coordinated transmit beamforming for multi-antenna network integrated sensing and communication," *arXiv preprint arXiv:2211.01085*, 2022.
- [32] M. A. Richards, J. Scheer, and W. A. Holm, *Principles of Modern Radar: Basic Principles*. New York, NY, USA: Scitech, 2010.
- [33] E. Björnson, J. Hoydis, and L. Sanguinetti, "Massive MIMO networks: Spectral, energy, and hardware efficiency," *Foundations and Trends® in Signal Processing*, vol. 11, no. 3-4, pp. 154–655, 2017.
- [34] D. Shiu, G. Foschini, M. Gans, and J. Kahn, "Fading correlation and its effect on the capacity of multielement antenna systems," *IEEE Trans. Commun.*, vol. 48, no. 3, pp. 502–513, 2000.
- [35] S. Guruacharya, B. K. Chalise, and B. Himed, "MAP ratio test detector for radar system," *IEEE Trans. Signal Process.*, vol. 69, pp. 573–588, 2020.
- [36] H. P. Benson, "Fractional programming with convex quadratic forms and functions," *European Journal of Operational Research*, vol. 173, no. 2, pp. 351–369, 2006.
- [37] G. Lanckriet and B. K. Sriperumbudur, "On the convergence of the concave-convex procedure," *Adv. in Neur. Inf. Proc. Sys.*, vol. 22, 2009.
- [38] 3GPP, "Further advancements for E-UTRA physical layer aspects (release 9)," *TS 36.814*, 2017.